; SUI-60-14)

A SATELLITE-BORNE MAGNETIC ELECTRON SPECTROMETER*

by

Curtis D. Laughlin (M.S. Thesis)

(NASA Contract NASw-17)

[7]

A thesis submitted in partial fulfillment of the requirements for the degree of Master of Science in the Department of Physics and Astronomy in the Graduate College of the State University of Iowa State U., Iowa City

August 1960 88p 19 ref

4658001

Chairman: Professor J. A. Van Allen

* This work was supported in part by the National Aeronautics and Space Administration.

ABSTRACT

This thesis describes the design, construction and calibration of satellite borne magnetic spectrometers for the measurement of the absolute intensity of electrons in a well defined energy interval, centered at about 50 kev. The three spectrometers of the final design were experimentally calibrated with various β-ray sources and with monoenergetic electrons from a small accelerator. Their geometric factors were about 2×10^{-5} cm^2 steradian for electrons in the energy range 45 to 55 kev. The geometric factors were less than 2% of this value for electrons of energy less than 40 kev or greater than 60 kev (but less than 10 Mev). The counting rate due to electrons, protons and other energetic ions capable of penetrating the 5.6 g/cm^2 shielding was determined by a geiger tube similar to the one in the spectrometer, similarly shielded and similarly located in the satellite assembly, but <u>not</u> provided with an entrance aperture.

One of the spectrometers was flown as a component of the S-46 payload on 23 March 1960. Due to failure of the high speed stages of the Juno II vehicular system the payload was not placed in orbit. During some 8 minutes of recorded flight data, the two geiger tubes operated properly, counting cosmic rays. The peak altitude of 370 km was not sufficient to permit measurement of a significant intensity of geomagnetically-trapped electrons.

A similar instrument is planned for a future satellite.

TABLE OF CONTENTS

Chapter		Page
I.	Introduction	1
II.	Design and Construction	3
III.	Calibration	16
	A. X-ray	16
	B. Electron Gun	18
	C. Beta Sources	35
IV.	Summary of Spectrometer Calibrations	44
V.	In-Flight Data	46
Appendix		50
References		52
Figure Captions		54

TABLE OF TABLES

Table No.		Page
1.	g' for Spectrometers 5 and 6 Computed from Electron Gun Data	25
2.	Summary of Beta-Source Information ...	36
3.	g_1' and g_{11}' for Three Spectrometers with Each of Three Beta-Ray Sources ...	41
4.	Summary of Spectrometer Calibrations ..	45
5.	In-Flight Data from Spectrometer No. 6	47

TABLE OF FIGURES

Figure No.		Page
1.	Assembly drawing of the magnetic spectrometer	57
2.	Representative electron trajectories in a spectrometer	58
3.	Field strength vs distance from uniform field	59
4.	Representative plateau curves for an Anton type 223 geiger tube	60
5.	Block diagram of the detectors and electronic components for satellite S-46	61
6.	Schematic drawing of the 700 v and 160 v DC power supplies for satellite S-46	62
7.	Schematic drawing for the detectors and preamplifiers for satellite S-46	63
8.	Schematic drawing of the scalers, logic circuits, and output amplifiers for detector C on satellite S-46	64
9.	Assembly drawing of the detector instrumentation package for satellite S-46	65

TABLE OF FIGURES (continued)

Figure No.		Page
10.	Photo of a completed detector assembly before potting	66
11.	Photo of a completed spectrometer prior to potting	67
12.	Photo of the component parts for a spectrometer	68
13.	r vs R for the spectrometer tube in spectrometer No. 5	69
14.	R_s/R_b vs Kv (X-ray) for spectrometer No. 5	70
15.	Experimental arrangement in the X-ray beam	71
16.	R_s/R_t vs Electron Energy for spectrometer No. 5 (semi-log plot) ...	72
17.	R_s/R_t vs Electron Energy for spectrometer No. 5 (linear plot)	73
18.	r_s vs θ for spectrometer No. 5	74
19.	Laboratory arrangement for the detection of bremsstrahlung produced in a thick target by monoenergetic electrons	75

TABLE OF FIGURES (continued)

Figure No.		Page
20.	Laboratory arrangement for the detection of bremsstrahlung produced in a thick target by monoenergetic electrons	76
21.	$r_s/N/\pi r^2$ vs Electron Energy	77
22.	f(E) vs E for a C^{14} beta-ray source ..	78
23.	Stray magnetic field about a spectrometer	79

I. INTRODUCTION

Since the discovery of the belts of geomagnetically trapped particles many experiments have been performed in an effort to identify the component particles and to determine their energy spectra.[1,2,3,4,5]

---

1. J. A. Van Allen, C. E. McIlwain, and G. H. Ludwig, "Radiation Observations with Satellite 1958 Epsilon", J. Geophys. Research 64, 271-286 (1959).

2. J. A. Van Allen, "The Geomagnetically-Trapped Corpuscular Radiation", J. Geophys. Research 64, 1683 (1959).

3. F. E. Holly and R. G. Johnson, "Composition of Radiation Trapped in the Geomagnetic Field at Altitudes up to 1,000 Kilometers", Air Force Special Weapons Center TN-59-15, March 1959.

4. F. E. Holly, "Radiation Measurements to 1,500 Kilometers with Atlas Pods", Air Force Special Weapons Center TR-60-9, May 1960.

5. M. Walt, L. F. Chase, Jr., J. B. Cladis, W. L. Imhof, "Energy Spectra and Altitude Dependence of Electrons Trapped in the Earth's Magnetic Field", to be published in Proceedings of the Cospar Space Science Symposium, North Holland Publ. Co., Amsterdam.

The magnetic spectrometer herein described was built in an attempt to obtain reliable and unambiguous data on the absolute intensity of electrons in a chosen and well known energy interval and to obtain such data comprehensively in space and time by prolonged flight of the spectrometer in a satellite orbit of high eccentricity.

II. DESIGN AND CONSTRUCTION

Satellite S-46 was proposed for the study of the origins and build-up and decay times of the radiation belts, correlation with solar activity and with geophysical phenomena, and determination of the composition of the radiation in the respective belts with particular emphasis on the very low energy components and on the energy spectrum of the electron component.[6] For this latter purpose it was decided that a magnetic spectrometer utilizing geiger tubes as detectors would be constructed.

The weight of the detector assembly with an electronics section consisting of two high voltage power supplies (160 v and 700 v), and an amplifier and scaling unit with logic and summing circuits for each of the five detectors to be carried was to be about six pounds, and was to be contained in a cylinder 5.5 inches in diameter. This section of

---

6. From a letter to L. H. Meredith by J. A. Van Allen, 22 October 1959 (unpublished).

the payload was to be designed and built at the State University of Iowa and would be powered by batteries and solar cells contained, with the telemetry subcarrier oscillators and transmitter, in a package constructed by the Army Ballistic Missile Agency. The main supply of power to the SUI assembly was to be provided at 6.5 v dc and was not to exceed 220 mw.

Operation of all detectors within a temperature range of -20° C to $+75^{\circ}$ C in vacuum was required -- the lower limit being set by the batteries and the upper limit by the transistors in the transmitter. They were to operate normally during and after a series of vibration tests including 20g RMS for 0.2 sec twice and 12g RMS for 7.8 sec twice with white noise in a bandwidth of 20-1500 cps; a spin test at 600 rpm for 3 min; longitudinal accelerations up to 35g in a centrifuge while the payload was spinning at 437 rpm about its axis; and a shock test of forty-five 25g impacts on a linear accelerator.

In order to obtain directly comparable measurements of the anisotropic radiation the various direction-sensitive detectors in S-46 were

oriented with their axes parallel. This common direction was parallel to the longitudinal axis of the cylindrical payload.

Anton type 223 end-window (1.2 mg/cm^2 mica) halogen quenched geiger tubes were chosen as detectors for the magnetic spectrometer because of their small active volumes and thin windows. The small active volume results in a low background counting rate from radiation entering the counter along paths other than those desired and the small overall size of the tubes makes possible an instrument small enough and light enough for satellite operation. Because the energy spectrum of trapped electrons apparently rises steeply at low energies it was desirable to detect electrons of the lowest energy practicable -- making the thin window necessary. It was decided to center the pass band of the spectrometer at about 50 kev and to make it about 10 kev wide. In this way a well defined "slice" of the spectrum (relatively free of absorption in the mica window) could be examined. Within this energy range about 80% of electrons

penetrate a 1.2 mg/cm^2 mica window.[7] Two detectors were used: one a background counter which, in addition to providing the necessary background correction for the other, the "spectrometer" tube, was valuable in its own right as a detector of penetrating radiation. To reduce the background rate each tube was surrounded by a 0.051 cm (0.4 g/cm^2) stainless steel sleeve encased in a lead cylinder with a 0.442 cm wall (5.0 g/cm^2), providing a total shielding of 5.4 g/cm^2 in addition to the magnesium spectrometer housing and the aluminum payload shell. See Fig. 1. The shielding was identical on both tubes with the exception of a slot 0.159 cm x 0.254 cm through the lead and stainless steel to the face of the spectrometer tube -- the size and shape of this slot having been determined by the computed focusing properties of the magnetic field and by the size

---

7. O. Huber, F. Humbel, H. Schneider, and A. de Shalit, "Spektrometrische Messung von β-β-Koinzidenzen", Helv. Phys. Acta 25, 3-34 (1952). Fig. 7, p. 20.

and location of the entrance apertures.

In addition to the two geiger tubes in the spectrometer, an additional geiger tube (Anton 213 or 302) was to be operated from the common 700 v power supply. With the nominal 6.5 v input the maximum current which could be drawn from this supply was 45 μa at 25° C. To avoid approaching this maximum it was necessary to use sufficient series resistance with each geiger tube to limit the current drawn whenever the tube was saturated due to high radiation intensity (or if one of the tubes should fail by going into continuous discharge). A resistance of 19.4 megohms was placed in series with each Anton 223 tube, thus limiting the current through it to 6.7 μa.

Because the proposed orbit would carry the spectrometer through the outer zone where the intensity of electrons with energy greater than 30 kev would be expected[2] to reach $10^{11} cm^{-2} sec^{-1}$ it was necessary that the geometric factor be small enough to assure that the geiger tube detector would not be operating near its maximum rate over

large portions of the orbit, with consequent loss of precision in determining the true rate. The maximum usable true rate was found experimentally to be of the order of 10^5 per sec for the Anton 223. (See Section III A.)

If a differential number-energy spectrum proportional to E^{-5} is assumed, the fraction of the number of electrons with energy greater than 30 kev in the pass band may be estimated:

$$\frac{\int_{45}^{55} E^{-5}\, dE}{\int_{30}^{\infty} E^{-5}\, dE} \sim 10^{-1} .$$

Thus, one could expect omnidirectional fluxes in the pass band of the order of $10^{10}\text{cm}^{-2}\text{sec}^{-1}$ to be encountered by the satellite. Allowing a factor of 10 for unusual situations it is seen that the geometric factor should be of the order of

$$\frac{(10^5\text{sec}^{-1})(4\pi \text{ steradian})}{(10)(10^{10}\text{cm}^{-2}\text{sec}^{-1})} \sim 10^{-5}\text{cm}^2 \text{ ster},$$

assuming for this estimate that the radiation is isotropically distributed.

A three piece aperture assembly was used. It consisted of an outer opening of 0.081 cm diameter, an inner opening of 0.109 cm diameter, and a baffle roughly midway between them with a hole of 0.099 cm diameter. The inner and outer openings were spaced 0.915 cm apart, giving a nominal geometric factor of 5.8×10^{-5} cm^2 steradian.

A factor important to the performance of the instrument is, of course, the magnetic field configuration. To keep the efficiency for collection of electrons in the pass band as high as possible a double-focusing sector-shaped field was used.[8,9,10]

---

8. W. G. Cross, "Two-Directional Focusing of Charged Particles with a Sector-Shaped, Uniform Magnetic Field", Rev. Sci. Instr. 22, 717 (1951).

9. M. Camac, "Double Focusing with Wedge-Shaped Magnetic Fields", Rev. Sci. Instr. 22, 197 (1951).

10. M. Cotte, "Recherches sur L'Optique Electronique", Ann. Phys. 10, 333 (1938).

"Double-focusing" refers to the fact that the sector shape provides focusing in the median plane parallel to the pole faces while the fringe field causes focusing in a plane perpendicular to this and containing the "central ray" into the detector. Critical parameters here are the distances of the object (outer aperture opening) and image (detector tube face) from the respective edges of the uniform field and the angles made by the entering and exiting particle trajectories with the edges of the uniform field in the median plane. Cross[4] has these parameters plotted in such a manner as to make choice of a compromising set of them a simple matter.

Separation of the pole pieces, i.e., the gap, was made great enough to prevent electrons from scattering off the pole faces but still small enough so that the required field strength could be attained with a conveniently sized Alnico V slug. Optimum focusing, which requires that the gap be short in comparison with the path length in the uniform field, was not attained since the gap was 0.216 cm and the path length about 0.75 cm. The 1.270 cm cube of Alnico V used with the pole pieces was capable of producing 1500 gauss in the

center of the gap. Calibration of the completed instruments showed that 1050 gauss was sufficient for the desired pass band and this latter value was used in the final design. Armco ingot iron was used for the pole pieces, these being held in good contact with the machine-ground faces of the magnet slug by two brass screws.

Paths of electrons with energy near the center of the pass band which were originally traveling, respectively, along the axis of the aperture assembly and along the most unfavorable paths for focusing are shown in Fig. 2. Paths are also shown for electrons with energies at the edges of the pass band incident along the aperture axis. These paths were computed from measurements of the fringe field along the lines of the axis of the aperture assembly and the axis of the spectrometer tube. Fig. 3 is a plot of these measurements of field strength vs distance from the edge of the pole pieces. The gauss-meter used for this purpose (and for measuring the field in the gap also) was a Dyna-Empire Model D-855, manufactured by Dyna-Empire, Inc., Garden City, N.Y., the probe of which had a sensitive area only 0.061 cm in diameter.

However, the distances involved were small also, and these measurements may be in considerable error, particularly near the edge of the uniform portion where the magnitude of the fringe field varies greatly with small changes in position.

The magnet assembly provided some shielding of the solid angle visible to the spectrometer tube for radiation (including bremsstrahlung produced in the payload) with sufficient stopping power to penetrate the walls of the payload shell and spectrometer housing, but some small regions within this solid angle required the addition of lead shielding. The "hat shield" covers the opening seen through the magnet gap and the portion of the magnet slug seen by the spectrometer tube. The lead baffle between the magnet and the tube further protects from these same regions. It is threaded to reduce "piping" of electrons into the tube by multiple scattering.

Geiger tubes for use in the spectrometer were chosen on the basis of low plateau slope and small relative change in plateau characteristics with aging and temperature. The Anton 223 tubes used were pro-

vided with rhodium plated cathodes to improve their high temperature characteristics. Fig. 4 shows a representative set of characteristics determined for the spectrometer tube in unit No. 5. The slope of the room temperature plateaus generally fell within the range 15 to 30 per cent per 100 v. Tubes to be used in a unit were matched as closely as possible in regard to counting rate and plateau slope under standard conditions so that variation in the output of the 700 v supply would not affect the ratio of the counting rates importantly.

In the assembly of the instruments the gieger tubes were centered in the stainless steel sleeves by machined foam rings around their front portions, the cathodes having been insulated from the steel by formica washers. The stainless steel sleeves were then inserted into the lead shields, foam potting material poured in, and the lead caps put into place and secured by clamps until the foam had cured. With the shields aligned in the housing and held to the side plates with magnesium saddle blocks the region around the lead (except in the region containing the magnet) was potted also. The

foam potting material used in all cases was Eccofoam FP mixed ten parts to one part (by weight) of catalyst 12-6, both manufactured by Emerson and Cuming, Inc., Canton, Massachusetts. This procedure assured that the heavy lead pieces would retain their positions without damage to their surfaces during vibration testing or launching. To prevent movement of the magnet assembly the four screws holding it in place were coated with Hysol 6020 (Houghton Laboratories, Inc., N.Y.) before being tightened.

A block diagram of the S-46 detector assembly with its associated electronics is shown in Fig. 5, and the 700 v. power supply, pre-amplifiers, and scalers, logic, and output amplifiers are diagrammed in Figs. 6, 7, and 8, respectively. The triple output scalers allowed a very wide range of counting rates to be read from the received telemetry.

A completed flight unit detector assembly as shown in a cut-away drawing in Fig. 9 and in a photograph in Fig. 10 weighed 6.4 lb. and operated on 177 mw from the 6.5 v. supply. A completed spectrometer weighed about 20 oz. (575 gm) and measured approximately

10 cm x 7.6 cm x 2.5 cm. Figs. 11 and 12 show components and a partially assembled spectrometer.

Calibration of the completed assemblies showed a negligible variation in counting rate of the Anton 223 tubes for temperature ranging from -30° C to 75° C. Some of these tubes did show spurious counting during vibration testing, but unless they suffered actual physical damage such as breakage or loosening of the anode wires this effect seemed to have no influence on their subsequent operation.

A thorough discussion of S-46 instrumentation has been prepared by George H. Ludwig of this laboratory.[11]

---

11. George H. Ludwig, "The Development of a Corpuscular Radiation Experiment for an Earth Satellite", Ph.D. Dissertation (August 1960).

III. CALIBRATION

A. X-ray.

Because of the rate limitations of a geiger tube and allied circuitry, the observed counting rate r is not equal in general to the true rate R which would be expected with an ideal tube and circuit. In order to properly interpret data from the geiger tubes used, the relationship between r and R must be known -- both with the scaling circuits used in the electron gun calibrations (sec. III - B) and when assembled in the flight payloads.

The relation between R and r was found experimentally in an X-ray beam known to follow the inverse square law at distances between about 30 cm and 250 cm from the target. It was found that at low X-ray intensities the apparent counting rate was proportional to intensity. For these conditions the true rate was taken to be equal to the apparent rate. Then with a constant setting of the X-ray machine the intensity was varied by locating the tube at various distances from the

X-ray target. The corresponding true rates were calculated for each position by the inverse square law. After exhausting the dynamic range available at a given setting of the X-ray machine, the X-ray voltage was increased and the tube was relocated at a position where its apparent rate was less than the greatest rate previously reached. Hence the true rate was known. The procedure was then repeated as many times as necessary to cover the desired dynamic range. Fig. 13 shows a representative example of the resulting curves, this one being for the spectrometer tube in unit No. 5. As yet no simple equation has been found to fit these curves accurately over their entire lengths.

The X-ray beam also provided a means of checking the relative shielding of the two tubes in the spectrometer units. Fig. 14 is a graph of the ratio of the spectrometer tube rate R_s to the background tube rate R_b vs X-ray voltage for unit No. 5 set broadside to the beam, and Fig. 15 shows the experimental arrangement and serves to define the angles mentioned below. For values of $R_s/R_b < 10$

the statistical accuracy is $\leq \pm 3\%$ and for values of $R_s/R_b > 10$ the statistical accuracy is $\leq \pm 10\%$. Rough preliminary checks were made with the spectrometer front-on to the beam and over a range of azimuth ϕ and tilt θ from this position. The results of these measurements are also shown in Fig. 14, and it is seen that R_s/R_b is dependent upon the direction of incidence of the radiation. The import of these X-ray measurements is discussed in section III - B.

B. Electron Gun.

The energy pass band of each instrument was determined directly by bombardment with electrons of various energies from an electron gun. Because of the very small beam currents used (of the order of 10^{-14} amp) a geiger tube was used to measure the beam. To make matters simple the tube used for this purpose was another Anton type 223 mounted behind an entrance aperture assembly identical to that in the spectrometers. Thus when this tube was properly positioned in the beam its true rate after correction for the efficiency for detection of electrons and the transmission factor of the tube window, gave the

number of electrons per sec entering the spectrometer entrance aperture. This "test tube" was mounted in the vacuum chamber of the electron gun in such a way that it could be swung into the beam, being positioned correctly in relation to the spectrometer by an alignment block on the spectrometer top, and then swung away to allow the electron beam to enter the spectrometer. The major drawbacks of this system were the non-uniformity and wandering of the electron beam. However, with care and patience, fairly reliable and reproducible data were obtained. In Fig. 16 is shown a representative curve obtained from such data, again for spectrometer No. 5, and Fig. 17 is a smoothed linear plot made from Fig. 16. The ordinate is the ratio of the true rate of the spectrometer tube R_s to the true rate of the test tube R_t. At the center of the pass band, then, with the incident beam approximately parallel to the entrance aperture axis, roughly 1/4 of the electrons entering the aperture are counted by the detector. At least part of the inefficiency is due to the fact that the trajectories of the particles

in the pass band were significantly curved before reaching the inner opening of the aperture assembly, and, therefore, did not all pass through this opening. (Cf. Fig. 2.)

The width of the pass band for each instrument was taken as the width of the R_s/R_t vs Electron Energy curve at half-height and again unit No. 5 is a representative example with a pass band width of about 11 kev (between 44 and 55 kev). See Table 4 also.

Supplementary peaks (see Figs. 16 and 17) about 0.01 of the maximum height were noted on the high energy side of the pass band of each instrument tested -- and in one case on the low side also. Typically, these were only a few kev above or below the minima of the steeply falling or rising acceptance curve. The supplementary peaks were presumed to be due to scattering within the instrument (e.g., from the smooth sides of the opening in the lead spectrometer tube shield) but were not proven to be so caused.

The data for Fig. 16 were taken with the

electron beam incident parallel (as nearly as possible with a somewhat divergent and wandering beam) to the spectrometer entrance aperture axis. Some data were taken with the spectrometer tipped a few degrees about an axis perpendicular to both the axis of the entrance aperture assembly and the axis of the spectrometer tube. When tipped out of the zero degree position, i.e., the center of the electron beam parallel to the entrance aperture axis, the test tube could not be used, and, therefore, because of the fluctuations of the beam with time, this information was not thoroughly reliable but was of value.

Generally, the maximum acceptance by the spectrometer as shown in Fig. 18 for unit No. 5 occurred for electrons with energies within the pass band when the front (as shown in Fig. 15) of the instrument was tilted to $\theta \sim -3^{\circ}$. This is about what one would expect from inspection of the curvature of the trajectories within the aperture system. (Fig. 2.)

A geometric factor g may be defined for the spectrometer by the equation

$$j = \frac{R_s}{\epsilon g},$$

where j is the unidirectional particle flux within the energy pass band of the spectrometer at the position of the entrance aperture, R_s is the true counting rate of the spectrometer tube, and ϵ is the efficiency of the spectrometer for detection of electrons with energies in the pass band. It was not necessary to separate ϵ and g, so an effective geometric factor g' for the spectrometers was defined by

$$g' = \epsilon g.$$

g' may be determined from

$$g' = a\int_0^{\pi/2} 2\pi f(\theta) \sin\theta \, d\theta,$$

where a is the area of the outer opening of the entrance aperture assembly and θ is the angle that the path of an incident electron makes with the axis

of the entrance aperture assembly. $f(\theta)$ describes the variation in spectrometer acceptance as a function of θ.

The acceptance of the spectrometer for electrons incident along the axis of the entrance aperture assembly may be determined from data such as that in Figs. 16 and 17 by correcting the "test tube" rate R_t for the transmission factor[7] t of the geiger tube window and for the geiger tube efficiency (0.85) for the detection of beta-rays as given by the manufacturer. That is, $R_t/0.85t$ gives the number of electrons per second which pass through the aperture assembly with no magnetic field present and with the incident beam parallel to the aperture assembly axis.

Now,

$$f(\theta) = \left(\frac{R_s}{R_t} \right) (0.85t) \frac{R_s(\theta)}{R_s(0)} ,$$

where $R_s(0)$ and $R_s(\theta)$ are the counting rates of the spectrometer tube at a given electron energy with the spectrometer set at 0^o and θ^o, respectively, to the incident electron beam. Since the data such as

those shown in Fig. 18 were taken with θ varying in only one plane, rotational symmetry was assumed about the line representing the incident path for which R_s was a maximum for a given energy. With this assumption numerical integration of $\int_0^{\pi/2} f(\theta) \sin\theta \, d\theta$ for an electron energy near the center of the pass band allowed the determination of g'. Values of g' obtained in this manner for spectrometers 5 and 6 are shown in Table 1. Data for R_s as a function of θ were not taken with spectrometer No. 4. It is felt that the geometric factors computed in this way are at least within a factor of two of being true values for the instruments tested.

If the counting rates of the spectrometer tubes include significant contributions from penetrating radiation (e.g., bremsstrahlung produced within the payload) then there exists a possible ambiguity in the data received from the two tubes because of their different shielding for this type of radiation as evidenced in Fig. 14. For instance, it might be possible that the counting rate in each tube is due exclusively to bremsstrahlung from

Table 1

g' for Spectrometers 5 and 6
Computed from Electron Gun Data

$$g' = 2\pi a \int_0^{\pi/2} f(\theta) \sin \theta \, d\theta$$

Spectrometer	g' (cm^2 ster)
5	2.2×10^{-5}
6	1.4×10^{-5}

140 kev electrons. If the background tube rate is 1 per sec, then the 18.5 per sec rate observed in the spectrometer tube (see Fig. 14) might be interpreted falsely as 18.5 - 1 = 17.5 per sec due to electrons in the energy pass band.

A rough check to determine the magnitude of this effect was made by placing a spectrometer behind a 35 mg/cm^2 (extrapolated range for 150 kev electrons) aluminum foil in an electron beam. The electron current to the foil was measured with a VTE-2 Electrometer manufactured by Tullamore Electronics Laboratory, Chicago, Illinois. Fig. 19 is a diagram of the experimental situation in the laboratory.

Assuming isotropic emission of X-rays from the target,[12] which is "thick" for electrons but "thin" for X-rays, the counting rate R of the

---

12. For the quality of this assumption see: Helmuth Kulenkampff, Untersuchungen der kontinuierlichen Röntgenstrahlung dünner Aluminiumfolien, Annalen der Physik, 87, 597 (1928).

geiger tube will be given by

$$R = \frac{KNd\Omega}{4\pi} \quad ,$$

where N is the number of electrons per sec striking the target, $d\Omega$ is the solid angle subtended at the target by the geiger tube, K is a constant which depends on the target material, the target thickness, the material and thickness of the counter wall and the efficiency of the counter for X-rays. If a is the cross-section of the tube averaged over angle and r the distance from the target to the tube then

$$d\Omega = \frac{a}{r^2} \quad ,$$

and $$R = KN \left(\frac{a}{4\pi r^2} \right) = Ka \left(\frac{N}{4\pi r^2} \right) .$$

The flight situation is diagrammed in Fig. 20. Any small area dA of the satellite hull will be exposed to only one-half of the total solid angle (assuming the hull to be everywhere concave inward) for particles with insufficient energy to penetrate

the payload. Assuming an isotropically distributed unidirectional intensity j_o the relation (for this case) between J, the omnidirectional intensity per unit plane area, and J_o, the omnidirectional intensity for unit sphere, is

$$\frac{J}{J_o} = \left(\frac{1}{2}\right)\frac{\int_0^{2\pi}\int_0^{\pi/2} j_o \sin\theta \cos\theta \, d\theta \, d\phi}{\int_0^{2\pi}\int_0^{\pi/2} j_o \sin\theta \, d\theta \, d\phi} = \frac{1}{4} .$$

Here θ is the angle between the path of the incident particle and the normal to dA and ϕ is the azimuth angle made by the path of the incident particle with some set arbitrary direction.

Again assuming isotropic radiation of the bremsstrahlung, the true counting rate dR of a geiger tube within the satellite due to bremsstrahlung produced in electron impacts on dA is given by

$$dR = KJdA \frac{d\Omega}{4\pi} = KJdA \frac{a}{4\pi r^2} = KJa \frac{dA}{4\pi r^2} ,$$

where K is the same as before for the same thickness of the same target material and for the same geiger

tube, and $d\Omega$ is again the solid angle subtended by the tube at dA. Integrating over the entire surface S, the total true rate R due to electron impacts on the skin is

$$R = K\,Ja \int_S \frac{dA}{4\pi r^2} .$$

For ease in visualization this may be written

$$R = K\,Ja \int_S \sec\psi \; \frac{\cos\psi\, dA}{4\pi r^2} = K\,Ja \int_S \sec\psi \; \frac{d\omega}{4\pi} ,$$

where ψ is the angle between r and the normal to dA and ω is the solid angle subtended at the detector by dA.

Since $\int_S \sec\psi \; \frac{d\omega}{4\pi}$ is the value of

$\sec\psi$ averaged over the entire solid angle it is apparent that the value of the integral will always be greater than unity for the case outlined above. How much greater may be estimated from the particular shape of the satellite shell or calculated if the equation of the surface is known.

For example, if the satellite shell is a sphere of radius c and the geiger tube is mounted at a distance b from the center,

$$I = \int_S \frac{dA}{4\pi r^2} = \frac{c}{4b} \ln \left\{ \frac{\left[1 + \frac{b^2}{c^2} + 2\frac{b}{c}\right]}{\left[1 + \frac{b^2}{c^2} - 2\frac{b}{c}\right]} \right\} .$$

Evaluation shows that I increases slowly from unity (for $b/c = 0$) until the condition $b = c$ is approached. For $b = c$, I becomes infinite and, as b continues to increase, I again decreases, approaching zero as b becomes very large.

As another example, consider a right circular cylindrical shell of radius c and axial length L with the geiger tube mounted on the axis and a distance b from one of the end planes. Now

$$\int_S \frac{dA}{4\pi r^2} = \frac{1}{2} \arctan \left(\frac{L-b}{c}\right) + \frac{1}{2} \arctan \left(\frac{b}{c}\right)$$

$$+ \frac{1}{4} \ln \left[\left(\frac{c^2}{(L-b)^2} + 1 \right) \left(\frac{c^2}{b^2} + 1 \right) \right] .$$

As a representative case let $c = 2b = \frac{L}{4}$. Then

$$\int_s \frac{dA}{4\pi r^2} = 1.3.$$

On the basis of these examples it seems reasonable to assume that $\int_s \frac{dA}{4\pi r^2}$ is approximately unity for most practical cases.

Consequently, if the counting rate for a given electron energy in the laboratory is made equal to the flight value due to an isotropically distributed omnidirectional intensity J_o of electrons of the same energy

$$J_o = 4J \sim \frac{N}{\pi r^2},$$

with the accuracy of the approximation depending upon the location of the detector in the satellite and the shape of the satellite. The ratio of the number of counts per sec in the spectrometer tube (in the laboratory case) to $N/\pi r^2$ is plotted as a function of electron energy in Fig. 21. In these tests the background counter in the spectrometer showed no in-

crease in rate within the statistical accuracy of about 10% from its cosmic ray background rate of 0.011 $\pm$ 0.001 counts per sec. The spectrometer was mounted so that the electron beam (before striking the aluminum target) was incident approximately parallel to the axis of the entrance aperture assembly.

It is now possible to estimate the counting rate produced in the spectrometer tube by bremsstrahlung from a given intensity of electrons with a given spectral distribution. For example, assume that the spectrometer tube counts at a rate of one per sec, corresponding to a unidirectional intensity of electrons with energies between 45 and 55 kev of about 10^5 cm^{-2} sec^{-1} $ster^{-1}$. Then, in this example, for a differential number energy spectrum proportional to E^{-5} the isotropically distributed omnidirectional intensity J_o of electrons with energies between, say, 20 kev and 250 kev may be computed:

$$J_o = 4\pi \times 10^5 \frac{\int_{20}^{250} E^{-5}\, dE}{\int_{45}^{55} E^{-5}\, dE} \sim 7 \times 10^7 \text{ cm}^{-2} \text{ sec}^{-1}.$$

By means of data obtained with the X-ray machine at voltages up to 250 kev an extension of the curve in Fig. 21 may be estimated. Calling $\eta = R_s/N/\pi r^2$, the value of η averaged over the energy range 20 kev to 250 kev $(\bar{\eta})$ may be determined by numerical integration. The rate to be expected due to bremsstrahlung in this case is

$$R = J_o \bar{\eta} \sim (7 \times 10^7)\ (10^{-12}) \sim 10^{-4} \text{ sec}^{-1}.$$

The lower limit of the energy range (20 kev) was chosen here because little or no experimental information exists regarding the spectral distribution of geomagnetically trapped electrons at energies less than 20 kev. The 250 kev upper limit was taken because experimental evidence[2] indicates that the expected intensities of geomagnetically trapped electrons with energies greater than this are rela-

tively small and because this was the highest electron energy conveniently obtained in this laboratory.

If the above computations are performed with an assumed differential number energy spectrum proportional to E^{-3} (with other conditions as before), the counting rate in the spectrometer tube due to bremsstrahlung is seen to be

$$R = J_o \bar{\eta} \sim (2 \times 10^{7}) (3 \times 10^{-11}) \sim 10^{-3} \text{ sec}^{-1}.$$

For an assumed differential number energy spectrum proportional to E^{-2} this rate is

$$R = J_o \bar{\eta} \sim (10^{7}) (10^{-10}) \sim 10^{-3} \text{ sec}^{-1}.$$

These examples do not appear unreasonable in view of present knowledge of the spectral distribution of geomagnetically trapped electrons. Therefore, the effect of bremsstrahlung on the counting rate of the spectrometer tube is considered to be negligible.

C. Beta Sources.

Experimental data with 3 beta sources, $_{28}Ni^{63}$, $_{61}Pm^{147}$, and $_{6}C^{14}$ were also used to find the actual geometric factors of the instruments. These sources were disks 3.5 cm in diameter; thus, when placed close to the spectrometer aperture they more than filled the solid angle of acceptance. The Ni^{63} source had no protective covering but the Pm^{147} was covered by 0.001" of mica (about 7.5 mg/cm^2) and the C^{14} had a 0.001" Mylar window (about 3.5 mg/cm^2). Both the Pm^{147} and the C^{14} were 1 mc strength and the Ni^{63} was 0.1 mc when prepared in August 1959. Table 2 gives the above information in addition to the half-lives and the maximum beta-particle energy for each of these nuclides.

The relatively short half-life of the Pm^{147} required that a correction be applied to data taken with this source if the original activity was used.

All measurements using these sources were made at a pressure of 5 mm Hg or less to reduce losses by scattering and absorption in air.

Table 2

Summary of Beta-Source Information

Nuclide	Half-life[13] (years)	Max β[13] energy (kev)	Source Window	Strength (Aug., 1959) (mc)
$_{28}Ni^{63}$	85	65	None	0.1
$_{61}Pm^{147}$	2.6	229	~ 7.5 mg/cm^2 Mica	1
$_{6}C^{14}$	~ 5600	155	~ 3.5 mg/cm^2 Mylar	1

13. American Institute of Physics Handbook, McGraw-Hill Book Co., Inc. (1957).

Because no measured emission spectra were available for the sources as actually prepared the spectra were computed, starting with the emission spectrum for each of the three nuclides[14] and then making corrections for absorption[7] and energy loss[15] in the source windows and detector windows where necessary. Because no data were available concerning actual source thicknesses no corrections were attempted for this effect upon the spectra. Back-scattering[16] was assumed to increase the uni-directional intensity perpendicular to the surface of each source over the nominal value for one-half the total solid angle by 25 per cent for the C^{14} and

---

14. N.B.S., Tables for the Analysis of β Spectra, Applied Mathematics Series, 13, June 1952.

15. N.B.S., Circular 577, Energy Loss and Range of Electrons and Positrons (July 1956).

16. L. Yaffe, "Backscattering of Electrons into Geiger-Mueller Counters", Conference on Absolute β-Counting, N. R. C. Preliminary Report No. 8, p. 27 (October 1950).

35 per cent for the Pm^{147}. No correction was attempted for the degradation in energy of the backscattered radiation. The spectra were drawn as shown in Fig. 22 for the C^{14} source.

The unidirectional intensity j perpendicular to the surface of each source was determined as follows. Letting S represent the activity of the source (including the appropriate backscattering correction) and A the area of one side of the disk S/2A will be the number of disintegrations per sec per cm^2, assuming areal uniformity of distribution of activity. The unidirectional intensity perpendicular to the surface is then

$$j = \frac{S}{(2A)\ (2\pi)} = \frac{S}{4\pi A}\ cm^{-2}\ sec^{-1}\ ster^{-1}.$$

From this, the integral

$$\left[\int_{o}^{E_{max}} f(E)dE\right]_I$$

over the computed spectrum (curve I in Fig. 22) was normalized to represent j.

There are two partially independent methods of computing g' (as defined in section III-B) from the spectra of the beta-ray sources and the data obtained with these sources. One method uses the rate r_s of the spectrometer tube for each source with an assembled spectrometer and the spectral intensity emitted by the source within the spectrometer energy pass band. This latter quantity is

$$\left[\int_{E_1}^{E_2} f(E)dE\right]_{II}$$

where E_1 and E_2 refer, respectively, to the lower and upper limits of the energy pass band for a particular spectrometer. Now,

$$g_i' = \frac{r_s}{\left[\int_{E_1}^{E_2} f(E)dE\right]_{II}} .$$

The second method requires the counting rate r_a obtained for each source with the spectrometer

tube (before assembly into the spectrometer) placed close behind a facsimile entrance aperture assembly, the rate r_s as defined above (neither r_s nor r_a ever exceeded a few counts per sec, so these were taken as the true rates), the computed ratio

$$\frac{\left[\int_{o}^{E_{max}} f(E)dE\right]_{III}}{\left[\int_{E_1}^{E_2} f(E)dE\right]_{III}},$$

giving, for a particular source, the fraction of the emission which has sufficient energy to penetrate the tube window with energy in a pass band and the nominal geometric factor g_n of the entrance aperture assembly so that

$$g'_{11} = g_n \left(\frac{r_s}{r_a}\right) \frac{\left[\int_{o}^{E_{max}} f(E)dE\right]_{III}}{\left[\int_{E_1}^{E_2} f(E)dE\right]_{III}}.$$

Values of g' determined by these two methods are listed in Table 3, and may be compared with the values shown in Table 1 obtained from electron gun data.

Table 3

g_i' and g_{ii}' for Three Spectrometers with Each of Three Beta-Ray Sources

$$g_i' = \frac{r_s}{\left(\int_{E_1}^{E_2} f(E)\,dE\right)_{III}} \quad cm^2 \text{ ster}$$

$$g_{ii}' = \ln\left(\frac{r_s}{r_a}\right)\frac{\left(\int_{o}^{E_{MAX}} f(E)\,dE\right)_{III}}{\left(\int_{E_1}^{E_2} f(E)\,dE\right)_{III}} \quad cm^2 \text{ ster}$$

Source	Spectrometer No. 4		Spectrometer No. 5		Spectrometer No. 6	
	g_i'	g_{ii}'	g_i'	g_{ii}'	g_i'	g_{ii}'
Ni^{63}	1.5×10^{-5}	6.3×10^{-5}	0.68×10^{-5}	9.9×10^{-5}	1.2×10^{-5}	7.4×10^{-5}
Pm^{147}	1.1×10^{-5}	3.4×10^{-5}	0.85×10^{-5}	2.9×10^{-5}	1.5×10^{-5}	5.0×10^{-5}
C^{14}	1.1×10^{-5}	3.2×10^{-5}	0.75×10^{-5}	2.0×10^{-5}	1.3×10^{-5}	5.0×10^{-5}

The two methods using the beta sources depend upon the shapes of the spectra and the first method is also dependent upon knowledge of the source strengths. Both of these are affected to an undetermined extent by backscattering, source thickness, uniformity of source deposition, possible contamination of a source since manufacture, and uncertainties in the corrections applied for source window effects. There seem to be no strong reasons to prefer either g_i' or g_{i1}' over the other although g_{i1}' depends upon experimental data rather than upon the manufacturer's statement for the effective source strength. It might also appear that g_{i1}' would be somewhat less affected by the failure to correct the spectra for energy degradation in backscattering.

All the values of g_{i1}' derived from the Ni^{63} source were unacceptably large (efficiency greater than 100 per cent). This is believed due to the fact that the energy pass bands were near to the high energy tail of the Ni^{63} spectrum so that the

spectrum of the backscattered radiation may have added significantly to the radiation in the pass bands, effectively making r_s large in comparison with $\left[\int_{E_1}^{E_2} f(E)dE\right]_{III}$ in the equation for g_{ii}. None of the Ni^{63} values of g'_{ii} was used in determining the final geometric factor for each spectrometer.

Because of the reasons stated above it is felt that g'_i and g'_{ii} cannot be considered to represent the value of the geometric factor of a spectrometer to better than a factor of about three.

IV. SUMMARY OF SPECTROMETER CALIBRATIONS

Table 4 is a summary of the knowledge of each spectrometer's characteristics as determined by the calibration procedures discussed. The error figures shown for the energy pass bands are estimates based upon the scatter of the data from the electron accelerator. Values of g' listed for spectrometers 5 and 6 are averages of the values obtained with the electron gun and with the beta sources but weighted twice as heavily for the electron gun values as for the others. In the case of spectrometer No. 4 no electron gun data were available so g' for this spectrometer is an average of the values derived from the beta sources. The error figure associated with each value of g' is taken to include the values averaged.

Table 4

Summary of Spectrometer Calibrations

Spectrometer	B (gauss)	Energy Pass Band (kev)	Center of Pass Band (kev)	g' (cm^2 ster)
4	1000 ± 2 1/2 %	45.6 ± 1.5 to 55.7 ± 1.5	50 ± 1.5	(2.1 ± 1.5) x 10^{-5}
5	1050 ± 2 1/2 %	43.5 ± 1.0 to 54.7 ± 1.0	49 ± 1	(1.7 ± 1.2) x 10^{-5}
6	1050 ± 2 1/2 %	47.5 ± 1.0 to 56.5 ± 1.0	52 ± 1	(2.4 ± 2.6) x 10^{-5}

V. IN-FLIGHT DATA

At 1335/11.2 UT 23 March 1960 satellite S-46 containing such a spectrometer (No. 6) as previously described was launched from Cape Canaveral, Florida. An orbit was not achieved. However, an altitude of about 370 kilometers was attained and readable telemetry was received for a period of about eight minutes.

The altitude reached was too low for trapped radiation;[17] consequently it was assumed that the counting rates observed for the two geiger tubes in the spectrometer were due to cosmic rays only.

The observed rates for each of the tubes have been computed and are presented in Table 5. These rates are in reasonable agreement with previous measurements at similar altitudes and geographical

---

17. S. Yoshida, G. H. Ludwig, and J. A. Van Allen, "Distribution of Trapped Radiation in the Geomagnetic Field", J. Geophys. Research 65, 807-813 (March 1960).

Table 5

In-Flight Data from Spectrometer No. 6

Channel 3: Spectrometer Tube, 2^7 counts per cycle.
Channel 4: Background Tube, 2^3 counts per cycle.

Channel 3

Flip No.	Length of 1/2 Cycle (sec)	r (counts per sec)	Universal Time of Telemetered Flip 23 March 1960
1	255.5	0.25 ± 0.03	1339/35
2			1343/50.5

Channel 4

1	24.4	0.16	1336/12
2	8.5	.47	
3	12.2	.33	
4	22.6	.18	
5	25.4	.16	
6	18.9	.21	1337/45
7	20.5	.20	
8	22.4	.18	
9	15.9	.25	
10	28.4	.14	
11	12.8	.31	

Table 5 (continued)

12	39.1	.10	1339/43
13	10.8	.37	
14	27.2	.15	
15	18.4	.22	
16	31.5	.13	
17	11.4	.35	
18	30.5	.13	1342/01
19	12.5	.32	
20	14.6	.27	
21	14.4	.28	
22	18.6	.21	
23	13.2	.30	
24	27.6	.14	1343/45
25			1344/13
1 - 25	481	0.20 $\pm$ 0.02	

position, e.g., the shielded (2.5 gm/cm^2 of lead and stainless steel) 302 counter on satellite 1958 ϵ exhibited a true rate between 1 and 2 counts per sec under similar conditions.[1] Since the omni-directional geometric factor for the type 223 geiger tube is about 0.195 of that for the 302,[18] one would have expected a rate of about 0.2 counts per sec to about 0.4 counts per sec assuming the radiation was hard enough to penetrate the 5.4 g/cm^2 shielding of the 223's. The observed rates for both tubes do lie in this range.

---

18. J. A. Van Allen, Private Communication (Notebook No. 15).

APPENDIX

Possible future use of instruments similar to the magnetic spectrometer in payloads containing other devices which might be affected by the magnetic field prompted the measurement of the "stray" field about a spectrometer. A proton precession magnetometer[19] was used for these measurements.

Fig. 23 shows the scalar magnitude (assuming the direction of the stray field vector to be known) of the stray field as measured in the plane of the spectrometer magnet assembly gap at two distances from the magnetometer. It is seen that the inverse cube relation holds for the observed values within the precision of the measurements:

$$\left(\frac{62\ \text{cm}}{98\ \text{cm}}\right)^3 = 0.25$$

$$\left(\frac{30\ \gamma}{115\ \gamma}\right) = 0.26$$

---

19. D. L. Chinburg, "Design, Construction, and Operation of a Proton Precession Magnetometer", M.S. Thesis and Research Report S.U.I. 60-6 (June 1960).

A spectrometer employing two magnet assemblies and two spectrometer tubes in one unit has been designed. The spectrometer tubes in this unit face in opposite directions, allowing the magnets to be arranged with their moments opposing. In this case the construction of the two magnet assemblies is identical but the fields in the gaps are in the approximate ratio 3:2. The spacing between centers is about 8 cm, so one would expect a null in the stray field along the line joining the magnets at about a distance x from the weaker magnet given by

$$\left(\frac{x}{x+8}\right)^3 = \frac{3}{2}$$

$$x \sim 65 \text{ cm.}$$

Such an assembly has been checked with the magnetometer at a distance of about 70 cm for this case, and the stray field determined to be of the order of 2γ.

REFERENCES

1. J. A. Van Allen, C. E. McIlwain, and G. H. Ludwig, "Radiation Observations with Satellite 1958 Epsilon", J. Geophys. Research 64, 271-286 (1959).

2. J. A. Van Allen, "The Geomagnetically-Trapped Corpuscular Radiation", J. Geophys. Research 64, 1683 (1959).

3. F. E. Holly and R. G. Johnson, "Composition of Radiation Trapped in the Geomagnetic Field at Altitudes up to 1,000 Kilometers", Air Force Special Weapons Center TN-59-15, March 1959.

4. F. E. Holly, "Radiation Measurements to 1,500 Kilometers with Atlas Pods", Air Force Special Weapons Center TR-60-9, May 1960.

5. M. Walt, L. F. Chase, Jr., J. B. Cladis, W. L. Imhof, "Energy Spectra and Altitude Dependence of Electrons Trapped in the Earth's Magnetic Field", to be published in Proceedings of the Cospar Space Science Symposium, North Holland Publ. Co., Amsterdam.

6. From a letter to L. H. Meredith by J. A. Van Allen, 22 October 1959 (unpublished).

7. O. Huber, F. Humbel, H. Schneider, and A. de Shalit, "Spektrometrische Messung von β-β-Koinzidenzen", Helv. Phys. Acta 25, 3-34 (1952). Fig. 7, p. 20.

8. W. G. Cross, "Two-Directional Focusing of Charged Particles with a Sector-Shaped, Uniform Magnetic Field", Rev. Sci. Instr. 22, 717 (1951).

9. M. Camac, "Double Focusing with Wedge-Shaped Magnetic Fields", Rev. Sci. Instr. 22, 197 (1951).

10. M. Cotte, "Recherches sur L'Optique Electronique", Ann. Phys. 10, 333 (1938).

11. George H. Ludwig, "The Development of a Corpuscular Radiation Experiment for an Earth Satellite", Ph.D. Dissertation (August 1960).

12. For the quality of this assumption see: Helmuth Kulenkampff, Untersuchungen der kontinuierlichen Rontgenstrahlung dunner Aluminiumfolien, Annalen der Physik, 87, 597 (1928).

13. American Institute of Physics Handbook, McGraw-Hill Book Co., Inc. (1957).

14. N.B.S., Tables for the Analysis of β Spectra, Applied Mathematics Series, 13, June 1952.

15. N.B.S., Circular 577, Energy Loss and Range of Electrons and Positrons (July 1956).

16. L. Yaffe, "Backscattering of Electrons into Geiger-Mueller Counters", Conference on Absolute β-Counting, N. R. C. Preliminary Report No. 8, p. 27 (October 1950).

17. S. Yoshida, G. H. Ludwig, and J. A. Van Allen, "Distribution of Trapped Radiation in the Geomagnetic Field", J. Geophys. Research 65, 807-813 (March 1960).

18. J. A. Van Allen, Private Communication (Notebook No. 15).

19. D. L. Chinburg, "Design, Construction and Operation of a Proton Precession Magnetometer", M.S. Thesis and Research Report S.U.I. 60-6 (June 1960).

FIGURE CAPTIONS

Fig. 1. Assembly drawing of the magnetic spectrometer.

Fig. 2. Trajectories of some representative electrons with energies in the energy pass band of spectrometer No. 6.

Fig. 3. Field strength vs. distance from the edge of the uniform field measured along the axis of the entrance aperture assembly and the axis of the detector.

Fig. 4. Representative plateau curves for an Anton type 223 geiger tube.

Fig. 5. Block diagram of the detectors and electronic components for satellite S-46.
(Courtesy of G. H. Ludwig.)

Fig. 6. Schematic drawing of the 700 v and 160 v DC power supplies for satellite S-46.
(Courtesy of G. H. Ludwig.)

Fig. 7. Schematic drawing of the detectors and preamplifiers for satellite S-46.
(Courtesy of G. H. Ludwig.)

Fig. 8. Schematic drawing of the scalers, logic circuits, and output amplifiers for detector C (the spectrometer tube) on satellite S-46.
(Courtesy of G. H. Ludwig.)

Fig. 9. Assembly drawing of the instrumentation package for satellite S-46.
(Courtesy of G. H. Ludwig.)

FIGURE CAPTIONS (continued)

Fig. 10. Photo showing a completed detector assembly (with power supplies and pre-amplifiers) before potting for satellite S-46. (Courtesy of G. H. Ludwig.)

Fig. 11. Photo of a completed spectrometer prior to potting.

Fig. 12. Photo of the component parts for a spectrometer.

Fig. 13. Graph of the actual rate r vs the true rate R for the spectrometer tube in spectrometer No. 5.

Fig. 14. Graph of the ratio of the true rate R_s of the spectrometer tube to the true rate R_b of the background tube as a function of accelerating potential in an X-ray machine for spectrometer No. 5. Some points are shown for various orientations of the spectrometer in the X-ray beam. Fig. 15 serves to define the positional parameters.

Fig. 15. Experimental arrangement in the X-ray beam.

Fig. 16. A semi-log plot of the ratio R_s/R_t vs Electron Energy, where R_t is the true rate of an Anton type 223 geiger tube (the "test tube") behind a facsimile spectrometer entrance aperture assembly in a monoenergetic electron beam and R_s is the true rate of the spectrometer tube with the test tube removed from the beam.

Fig. 17. A smoothed linear plot made from Fig. 16.

FIGURE CAPTIONS (continued)

Fig. 18. Graph of the observed counting rate r_s of the spectrometer tube in spectrometer No. 5 as a function of the tilt angle θ (see Fig. 15) for various electron energies.

Fig. 19. Laboratory arrangement for the detection of bremsstrahlung produced in a target, thick for electrons but thin for X-rays, by monoenergetic electrons.

Fig. 20. Sketch used in computing the counting rate of a geiger tube within a satellite due to bremsstrahlung produced in the satellite shell.

Fig. 21. Graph of the number of counts per second in the spectrometer tube per electrons cm^{-2} sec^{-1} $(r_s/N/\pi r^2)$ as a function of electron energy for spectrometer No. 5. The spectrometer was mounted in correspondence with Fig. 19.

Fig. 22. f (E) vs E for a C^{14} beta-ray source, showing the effects of absorption and energy loss in the windows of the source and geiger tube.

Fig. 23. Measurements of the stray magnetic field about a spectrometer.

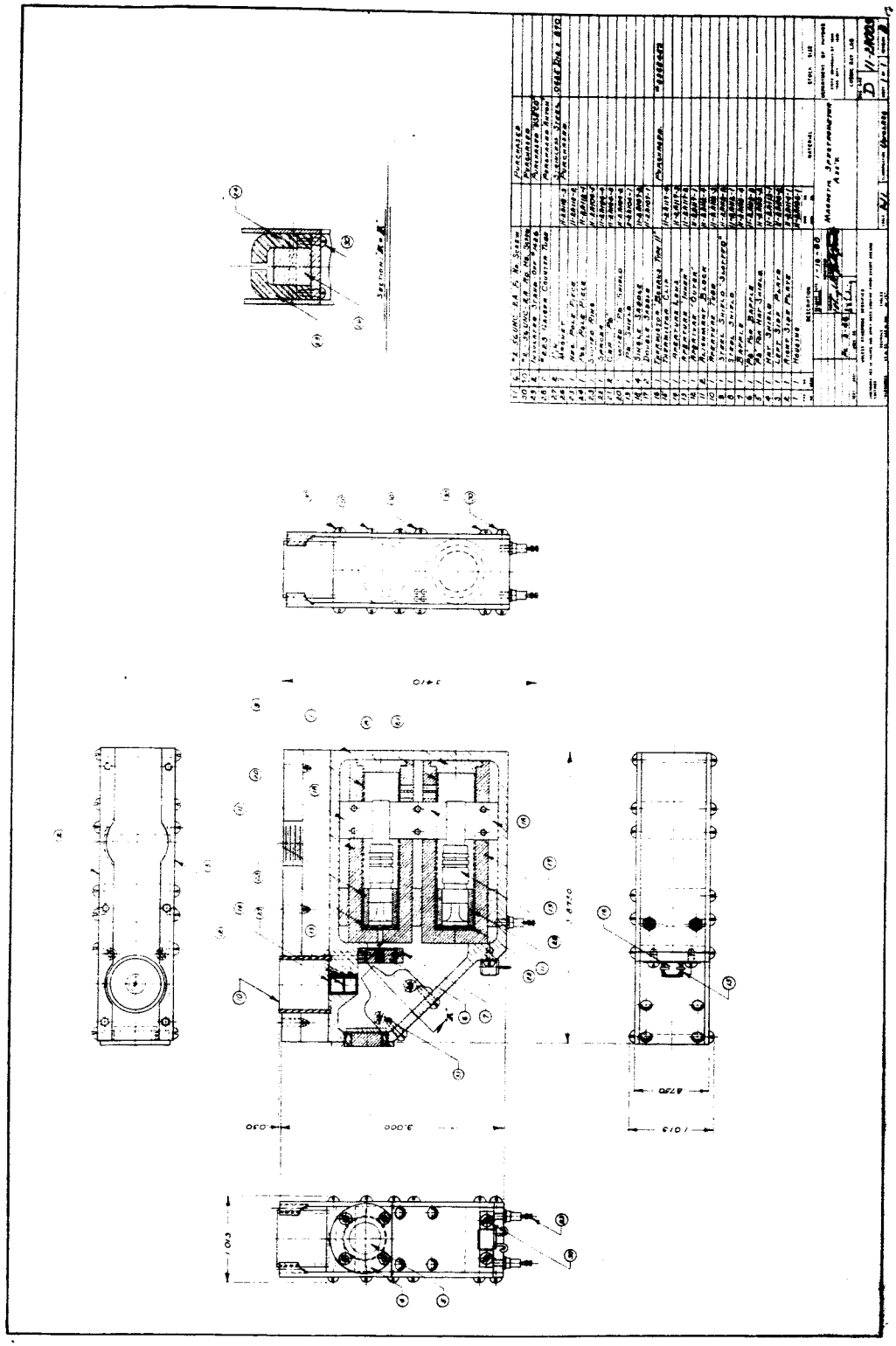

FIG. I

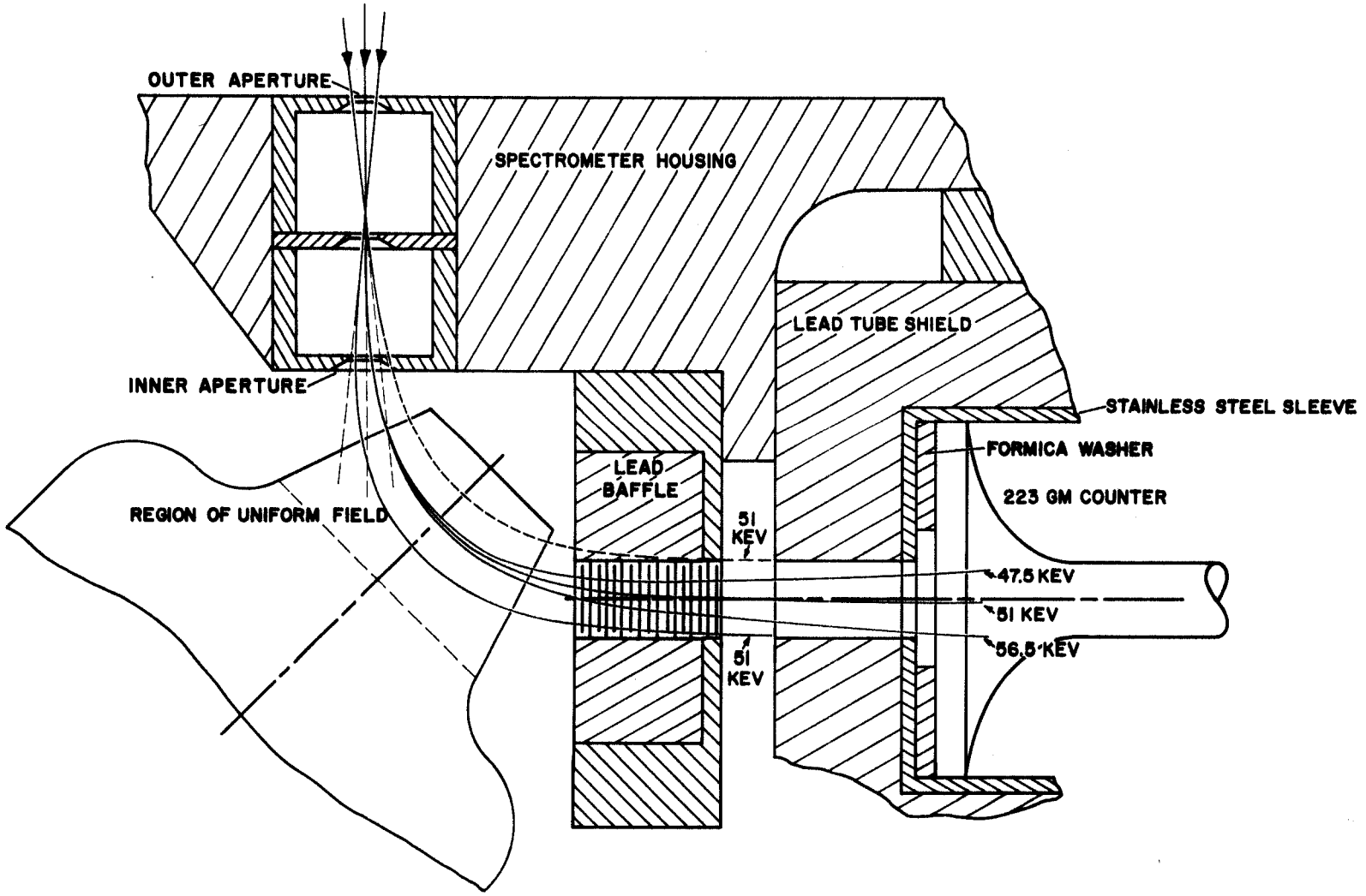

REPRESENTATIVE ELECTRON TRAJECTORIES IN SPECTROMETER WITH PASS BAND 47.5–56.5 KEV.

FIG. 2

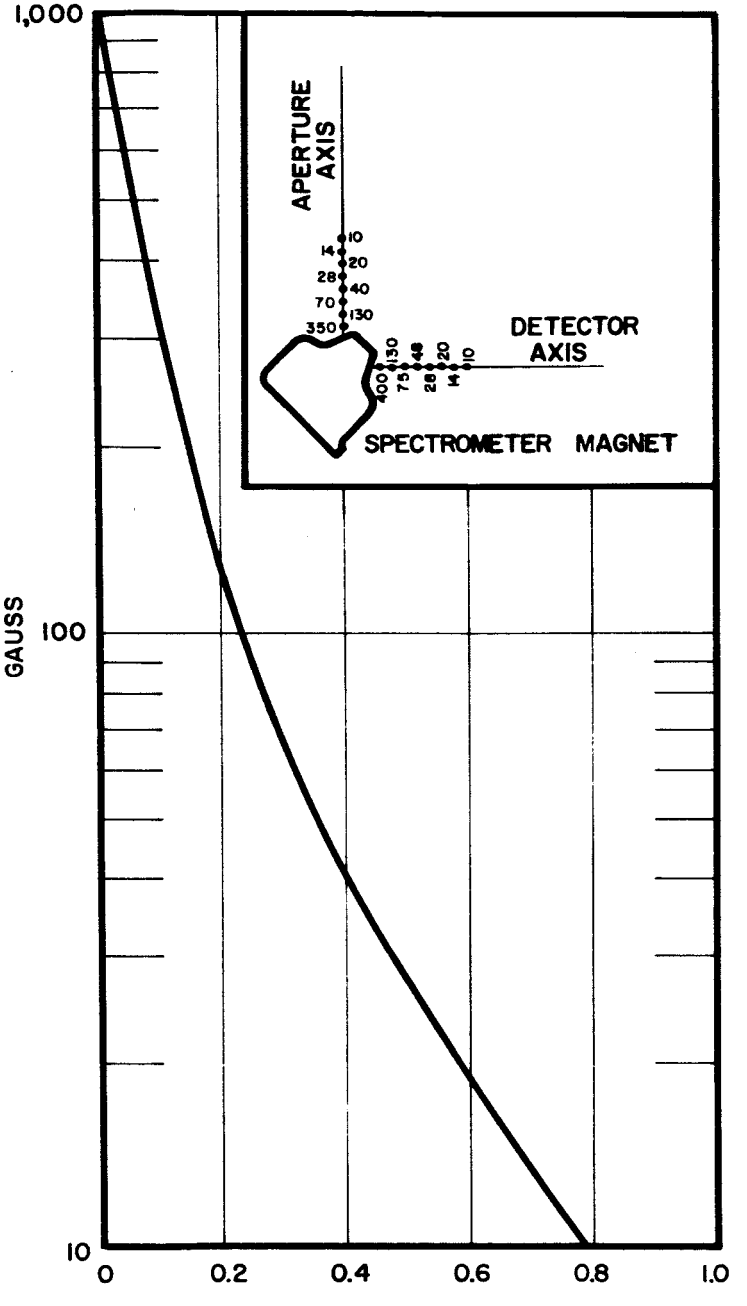

FIG. 3, FRINGING FIELD ALONG THE APERTURE AND DETECTOR AXES FOR A 1050 GAUSS SPECTROMETER MAGNET.

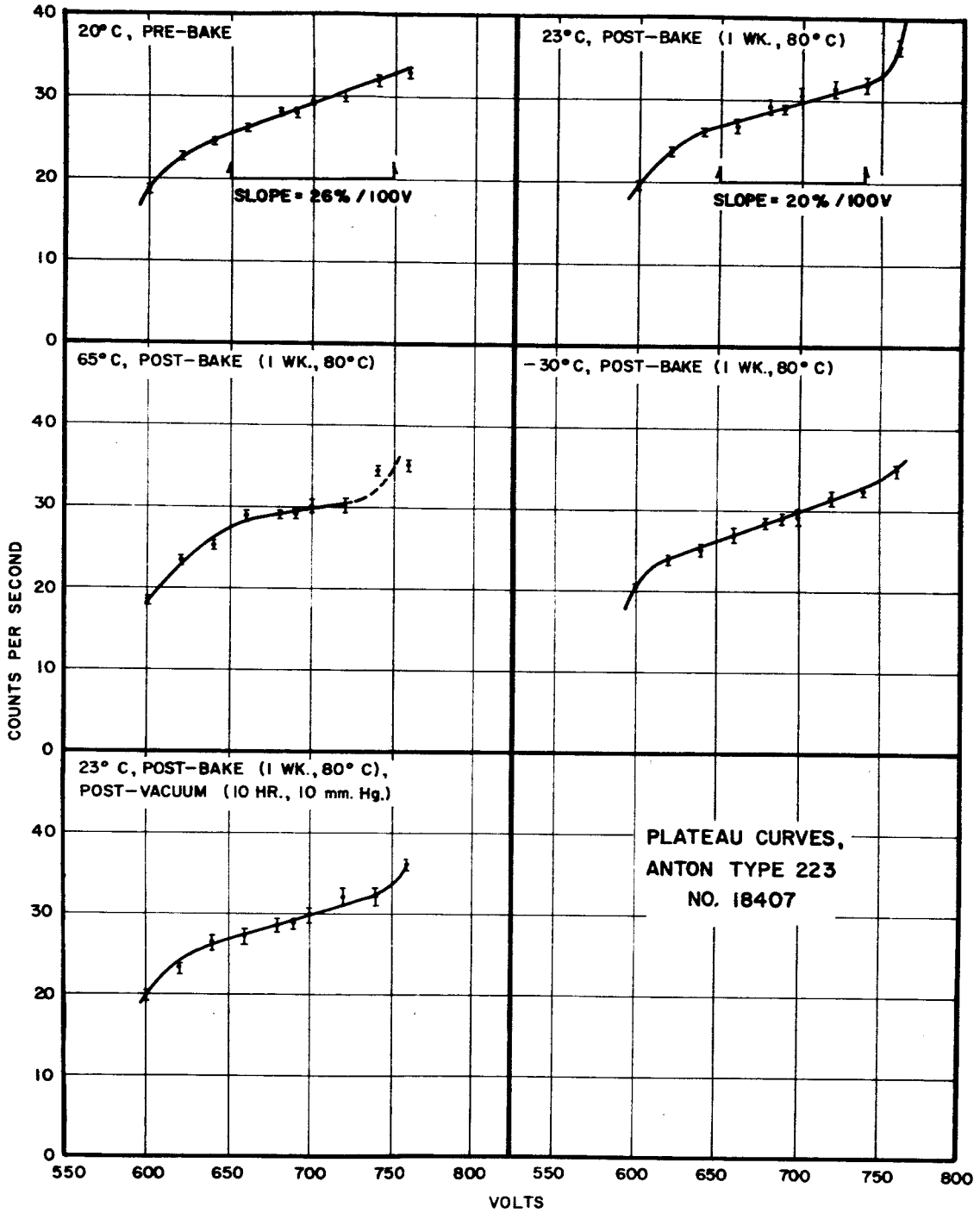
20° C, PRE-BAKE
SLOPE = 26% / 100V
23° C, POST-BAKE (1 WK., 80° C)
SLOPE = 20% / 100V
65° C, POST-BAKE (1 WK., 80° C)
-30° C, POST-BAKE (1 WK., 80° C)
23° C, POST-BAKE (1 WK., 80° C), POST-VACUUM (10 HR., 10 mm. Hg.)
PLATEAU CURVES, ANTON TYPE 223 NO. 18407
COUNTS PER SECOND
VOLTS
0
10
20
30
40
550
600
650
700
750
800

FIG. 4

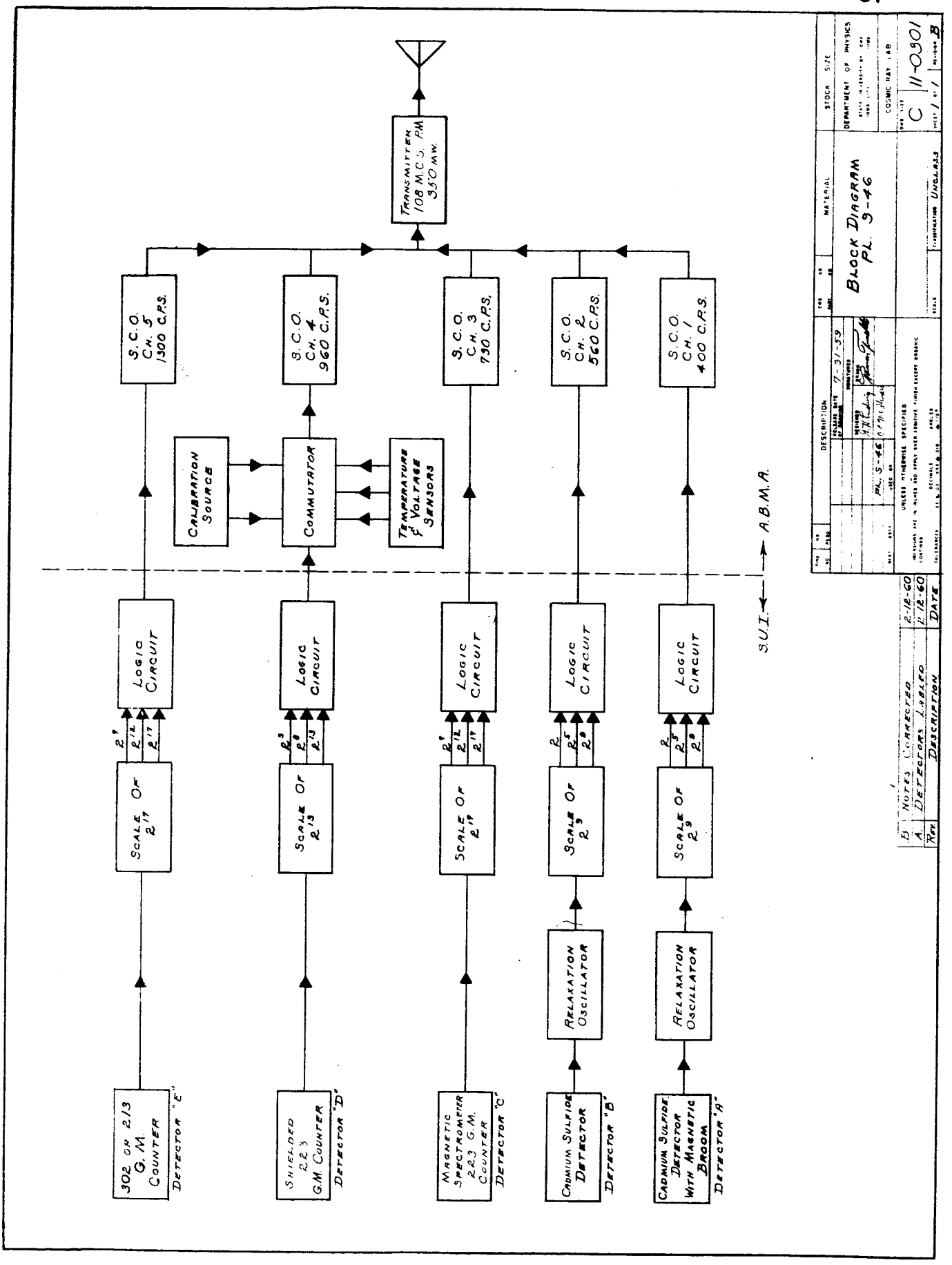
TRANSMITTER
108 M.C.S. P.M.
3.5 O MW.
S.C.O. CH. 5 1300 C.P.S.
S.C.O. CH. 4 960 C.P.S.
S.C.O. CH. 3 730 C.P.S.
S.C.O. CH. 2 560 C.P.S.
S.C.O. CH. 1 400 C.P.S.
CALIBRATION SOURCE
COMMUTATOR
TEMPERATURE & VOLTAGE SENSORS
A.B.M.A.
S.U.I.
LOGIC CIRCUIT
SCALE OF 2^17
SCALE OF 2^13
SCALE OF 2^19
SCALE OF 2^9
RELAXATION OSCILLATOR
302 OR 213 G.M. COUNTER
DETECTOR "E"
SHIELDED 223 G.M. COUNTER
DETECTOR "D"
MAGNETIC SPECTROMETER 223 G.M. COUNTER
DETECTOR "C"
CADMIUM SULFIDE DETECTOR
DETECTOR "B"
CADMIUM SULFIDE DETECTOR WITH MAGNETIC BROOM
DETECTOR "A"
BLOCK DIAGRAM PL. 3-46
DEPARTMENT OF PHYSICS
COSMIC RAY LAB
C 11-0901
NOTES
A. DETECTORS LABELED
B
REV
DESCRIPTION
DATE
2-12-60
2-12-60

FIG. 5

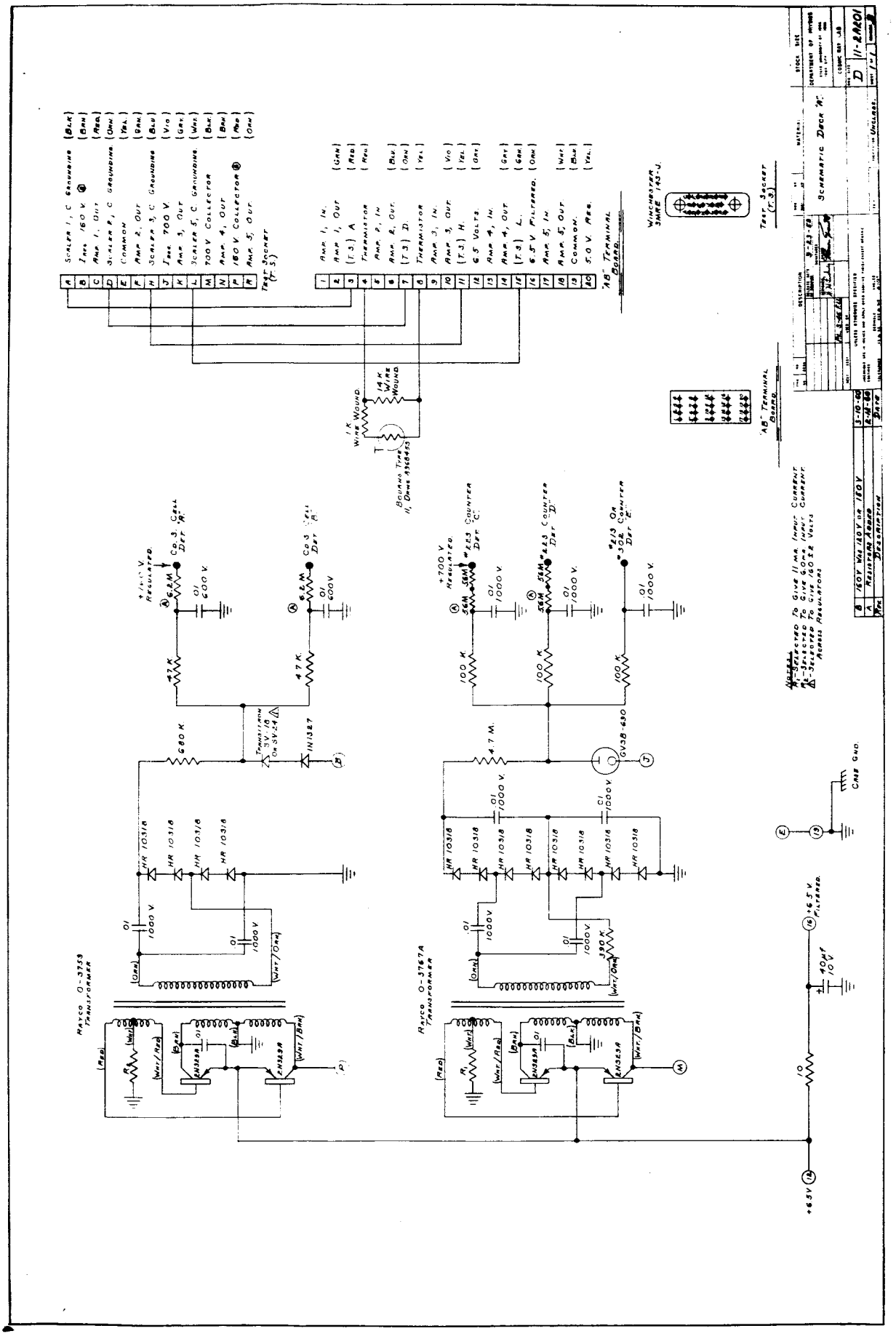

FIG. 6

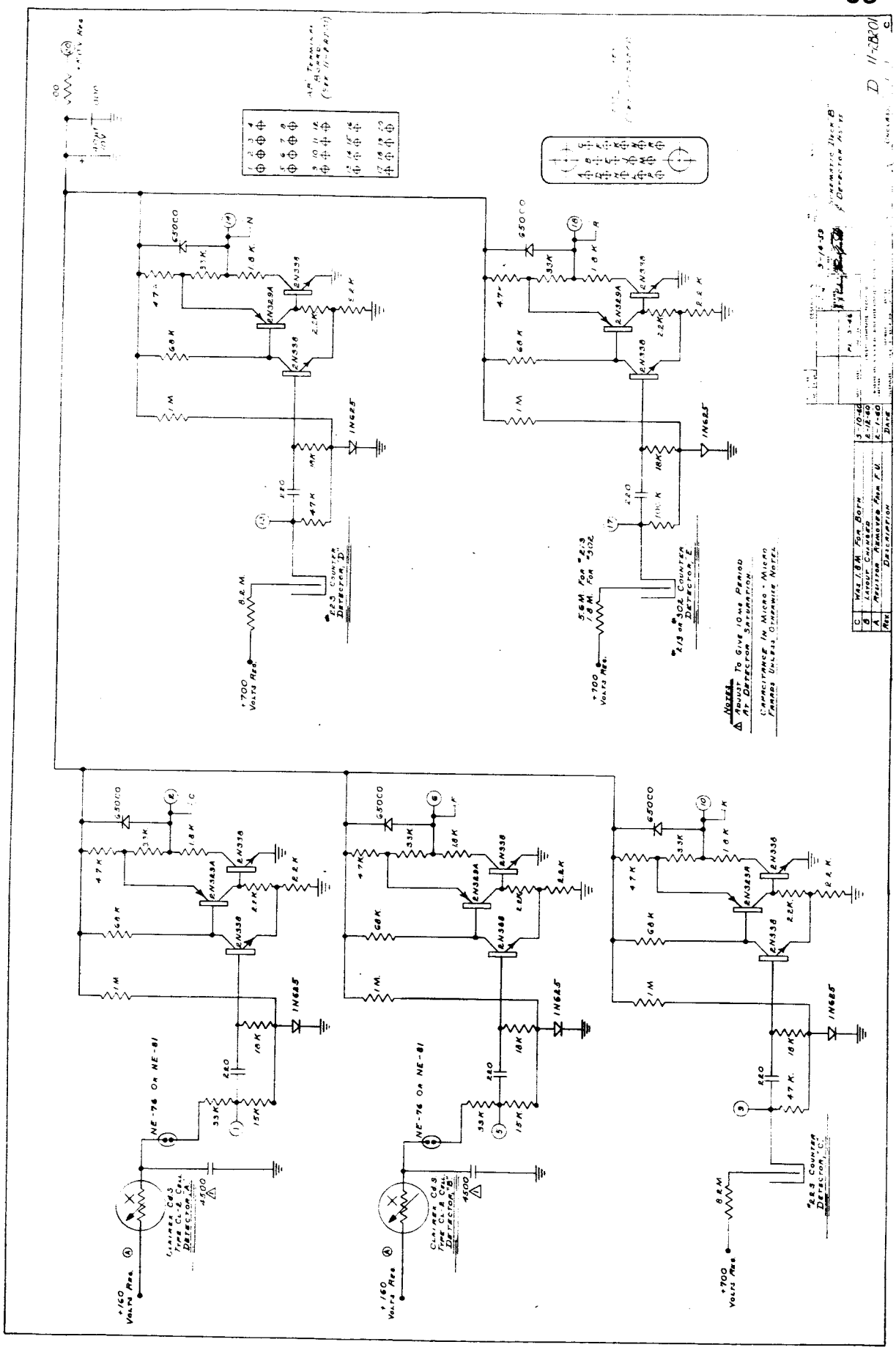

FIG. 7

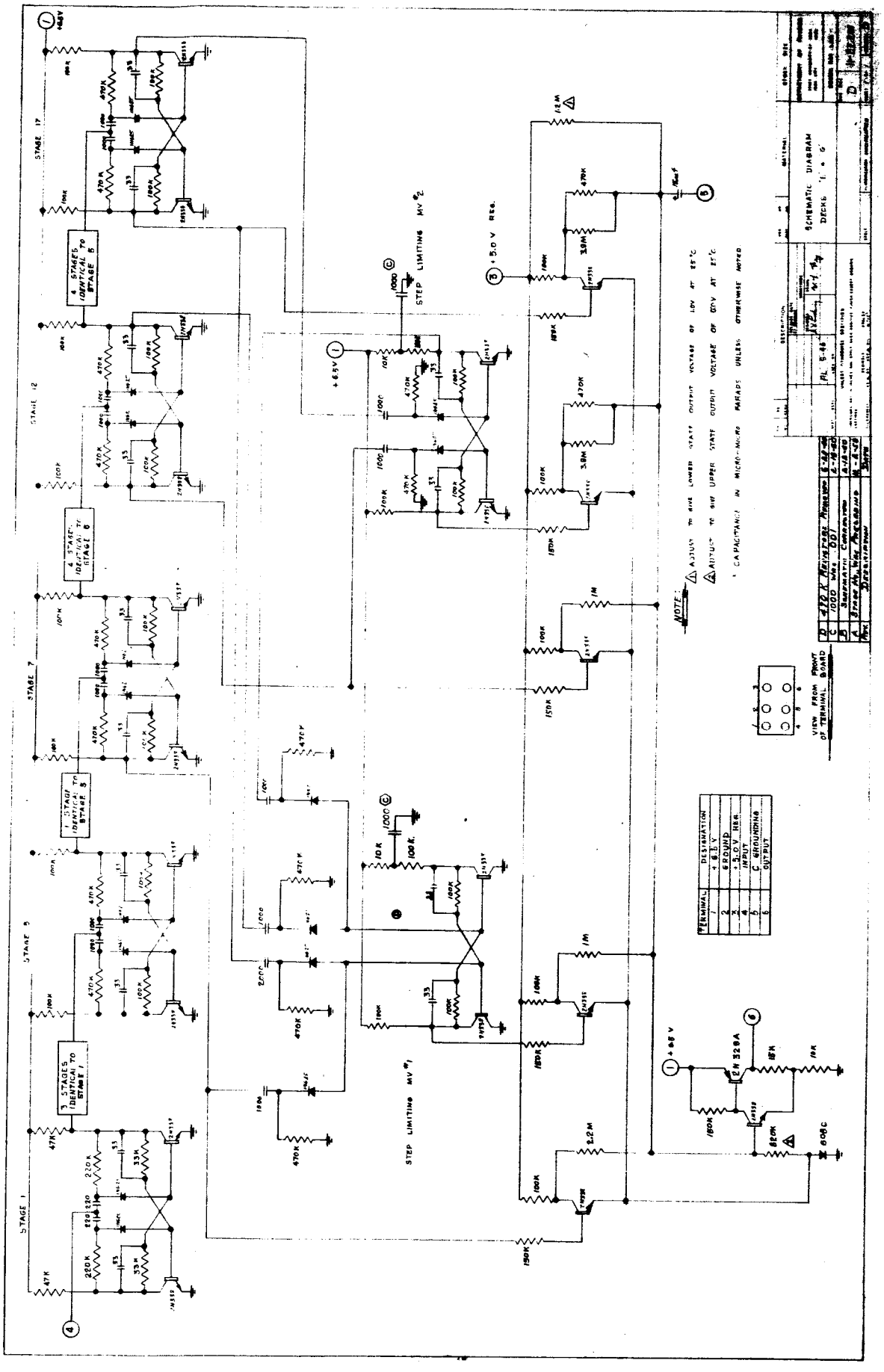
STAGE 12
STAGE 11
STAGE 10
STAGE 9
STAGE 8
STAGE 7
STAGE 6
STAGE 5
STAGE 4
STAGE 3
STAGE 2
STAGE 1
4 STAGES IDENTICAL TO STAGE 6
4 STAGES IDENTICAL TO STAGE 6
1 STAGE IDENTICAL TO STAGE 5
3 STAGES IDENTICAL TO STAGE 1
STEP LIMITING MV #2
STEP LIMITING MV #1
+6.5V
+5.0 V REG.
+6.5 V
2N 3638A
NOTE:
VIEW FROM FRONT OF TERMINAL BOARD
TERMINAL DESIGNATION
1 +6.5 V
2 GROUND
3 +5.0 V REG
4 INPUT
5 GROUNDING
6 OUTPUT
SCHEMATIC DIAGRAM
DECKS 1 + 6

FIG. 8

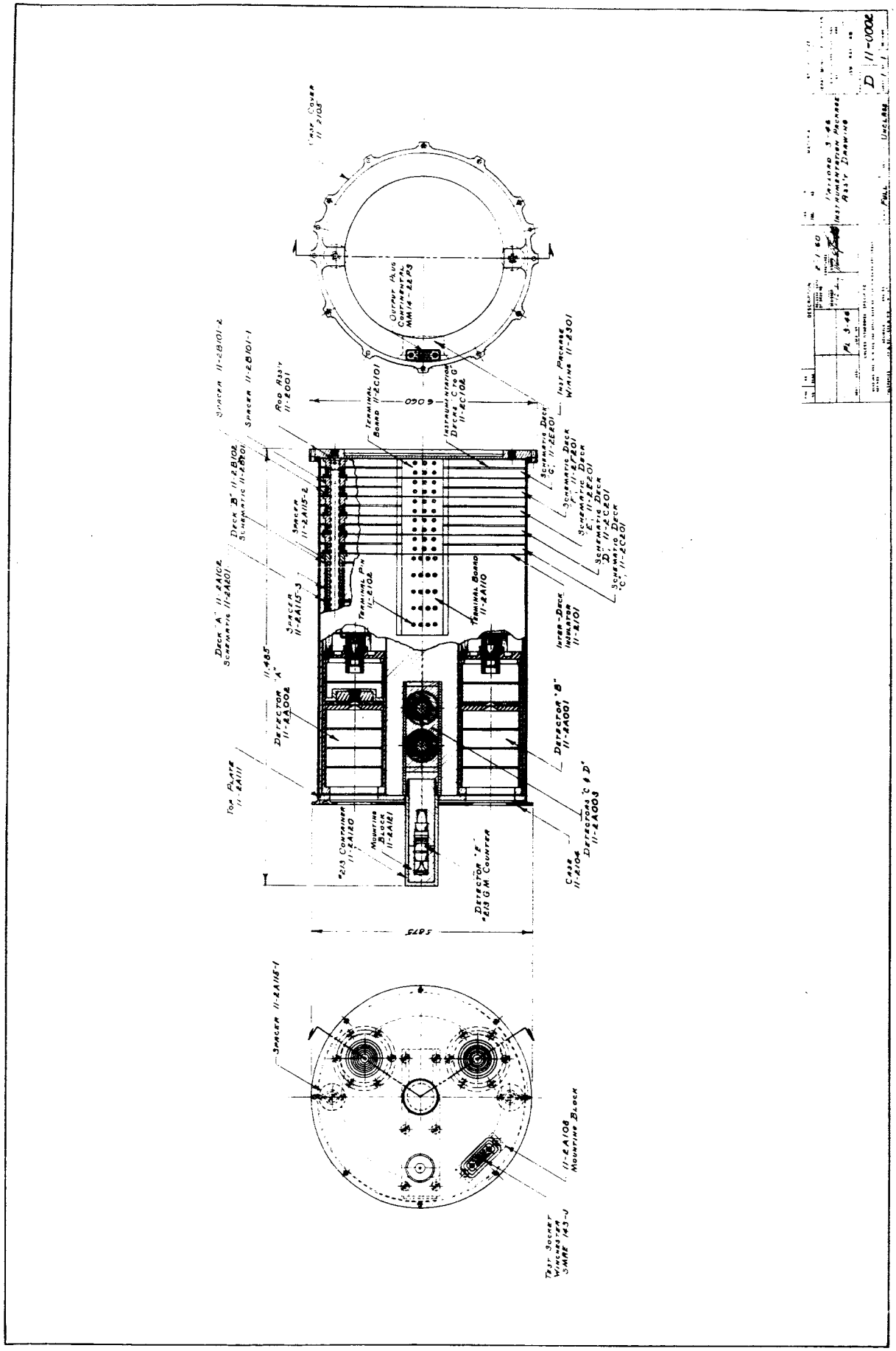

FIG. 9

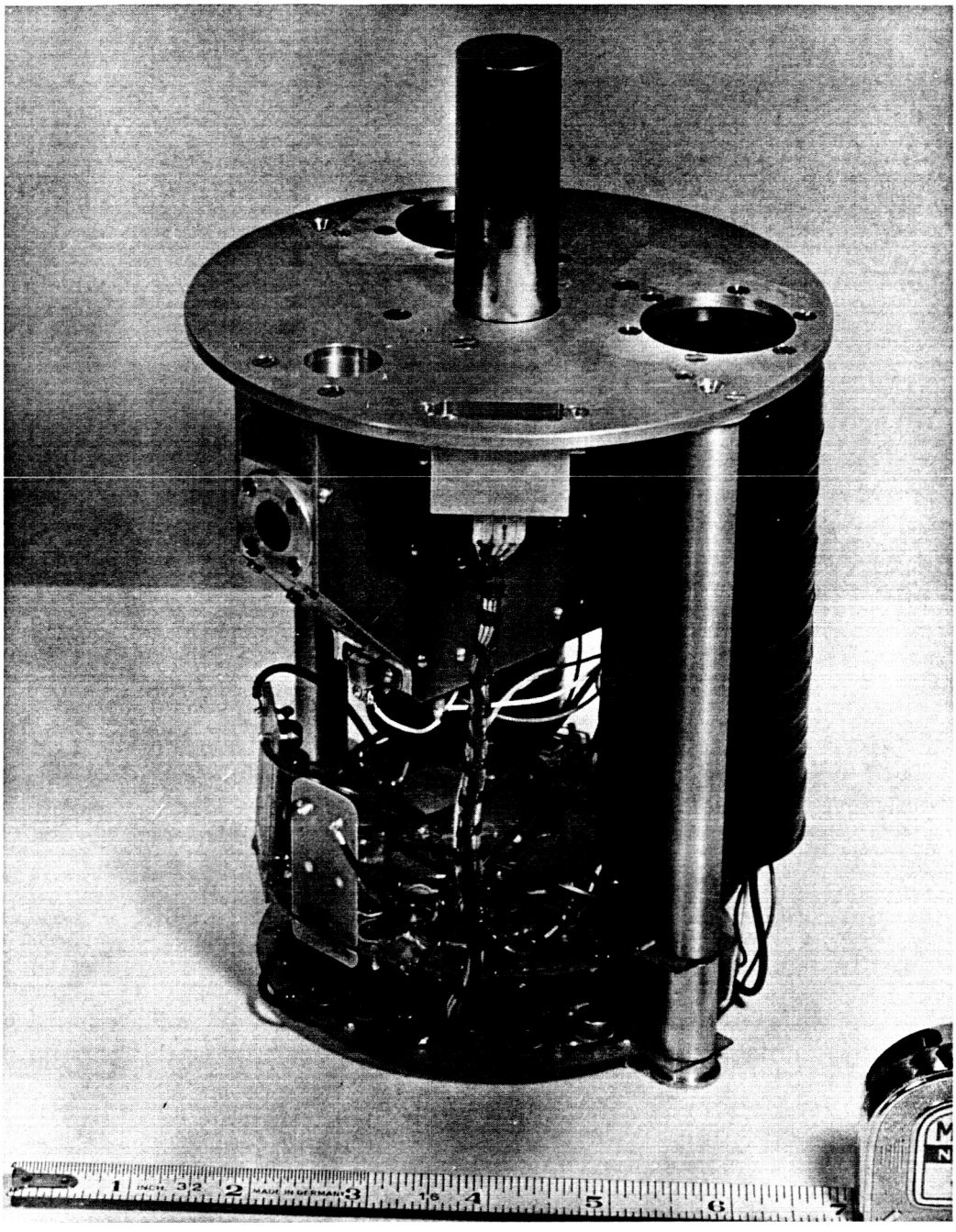

FIG. 10

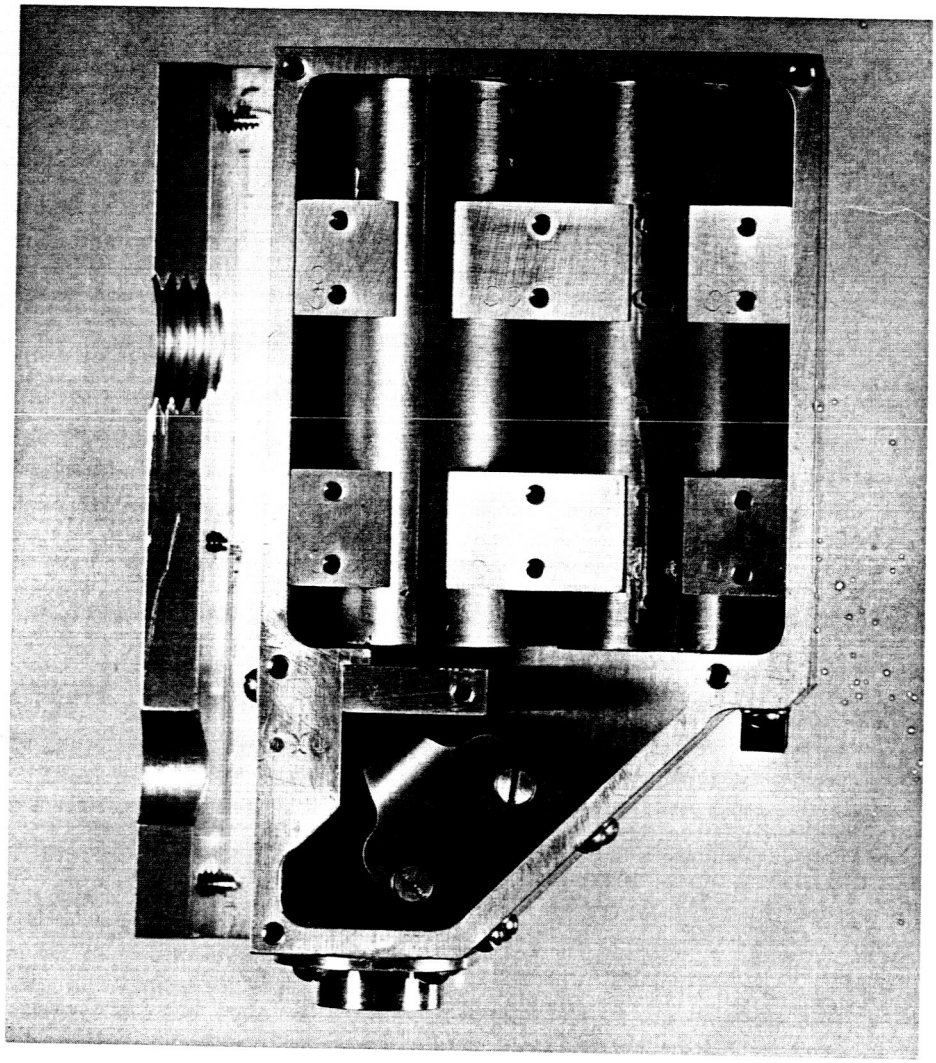

FIG. 11

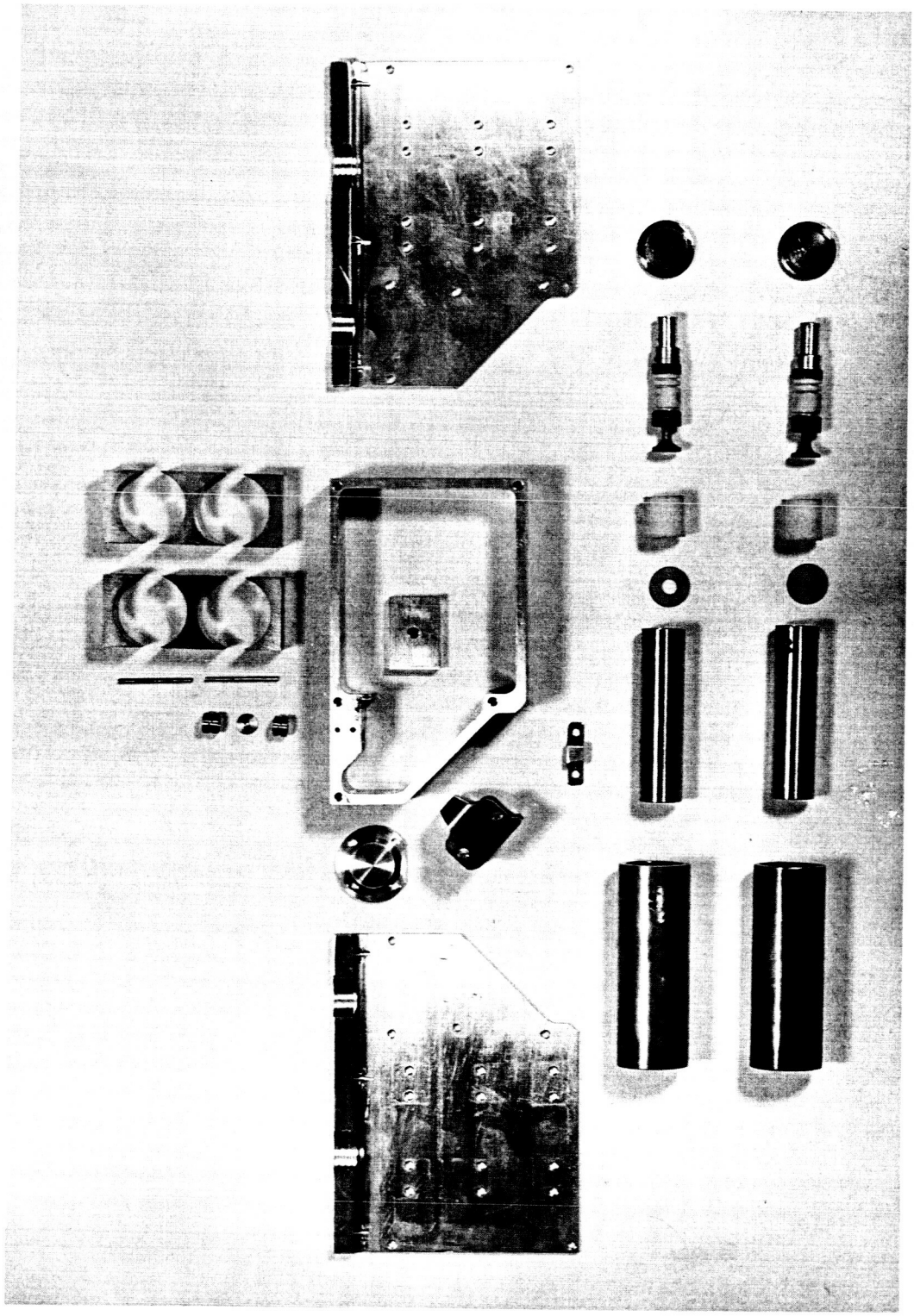

FIG. 12

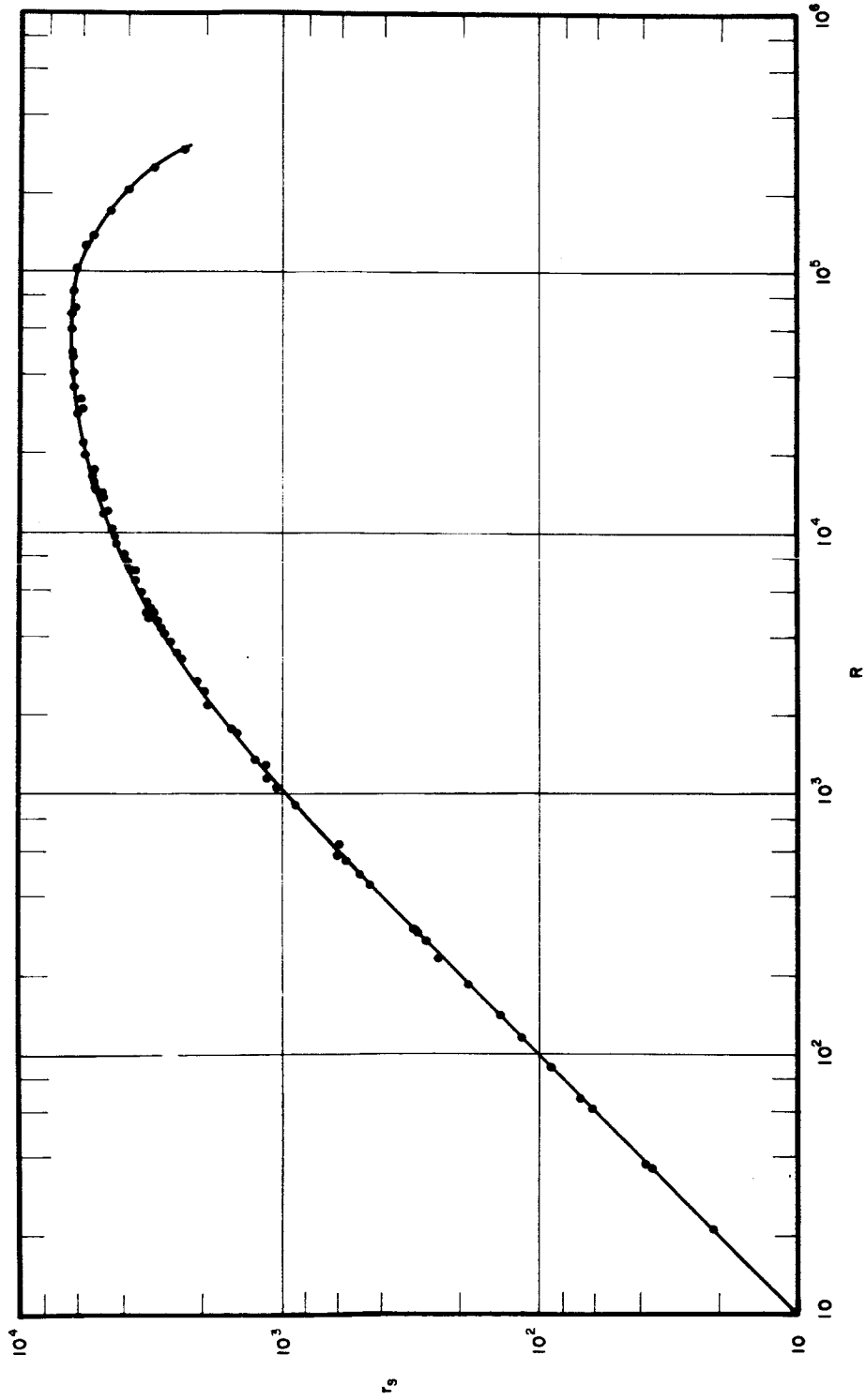

r VS. R FOR THE SPECTROMETER TUBE IN UNIT NO. 5

FIG. 13

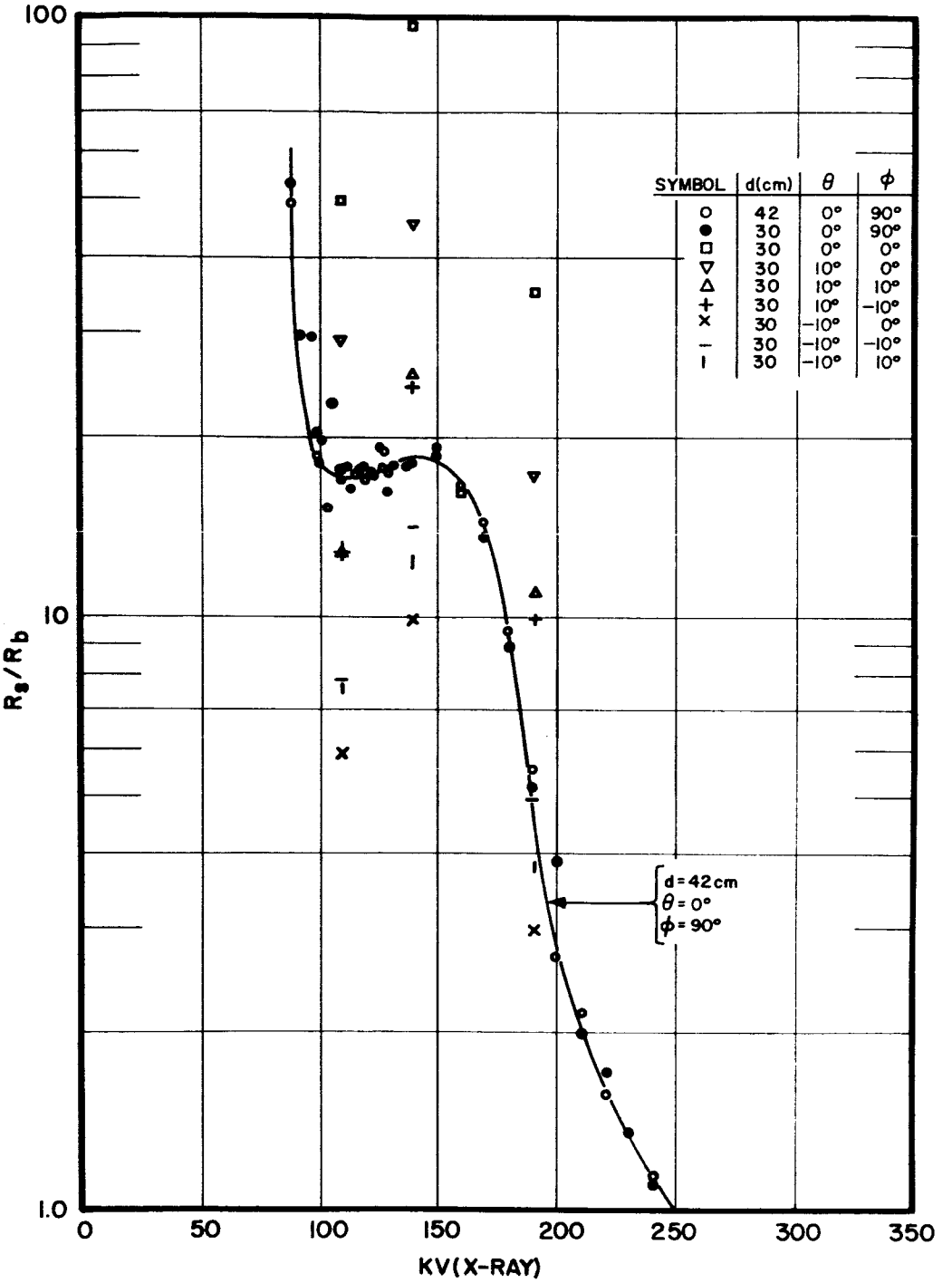

FIG. 14, R_s/R_b vs. X-RAY VOLTAGE FOR SPECTROMETER NO. 5

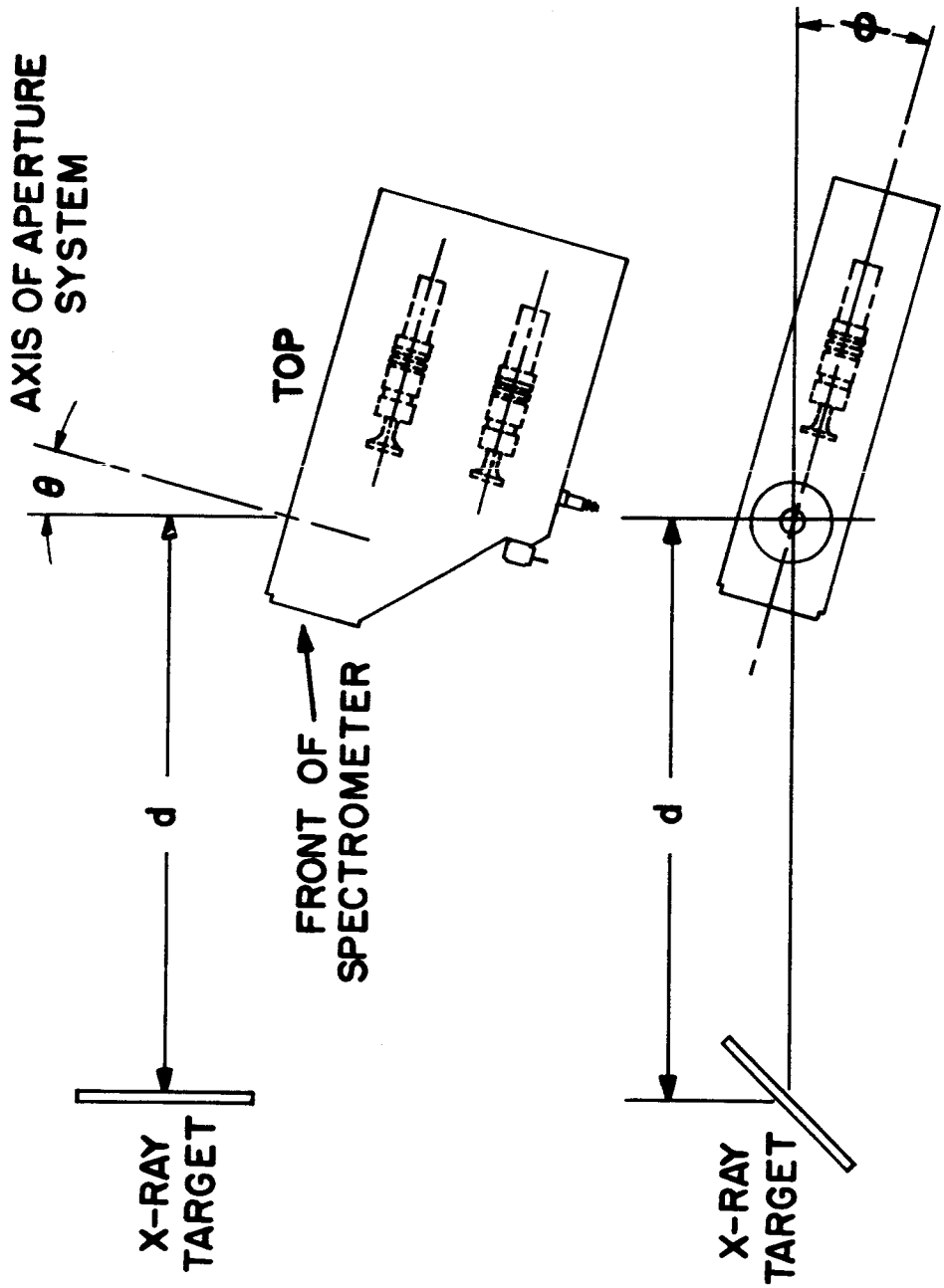

EXPERIMENTAL ARRANGEMENT IN X-RAY BEAM

FIG. 15

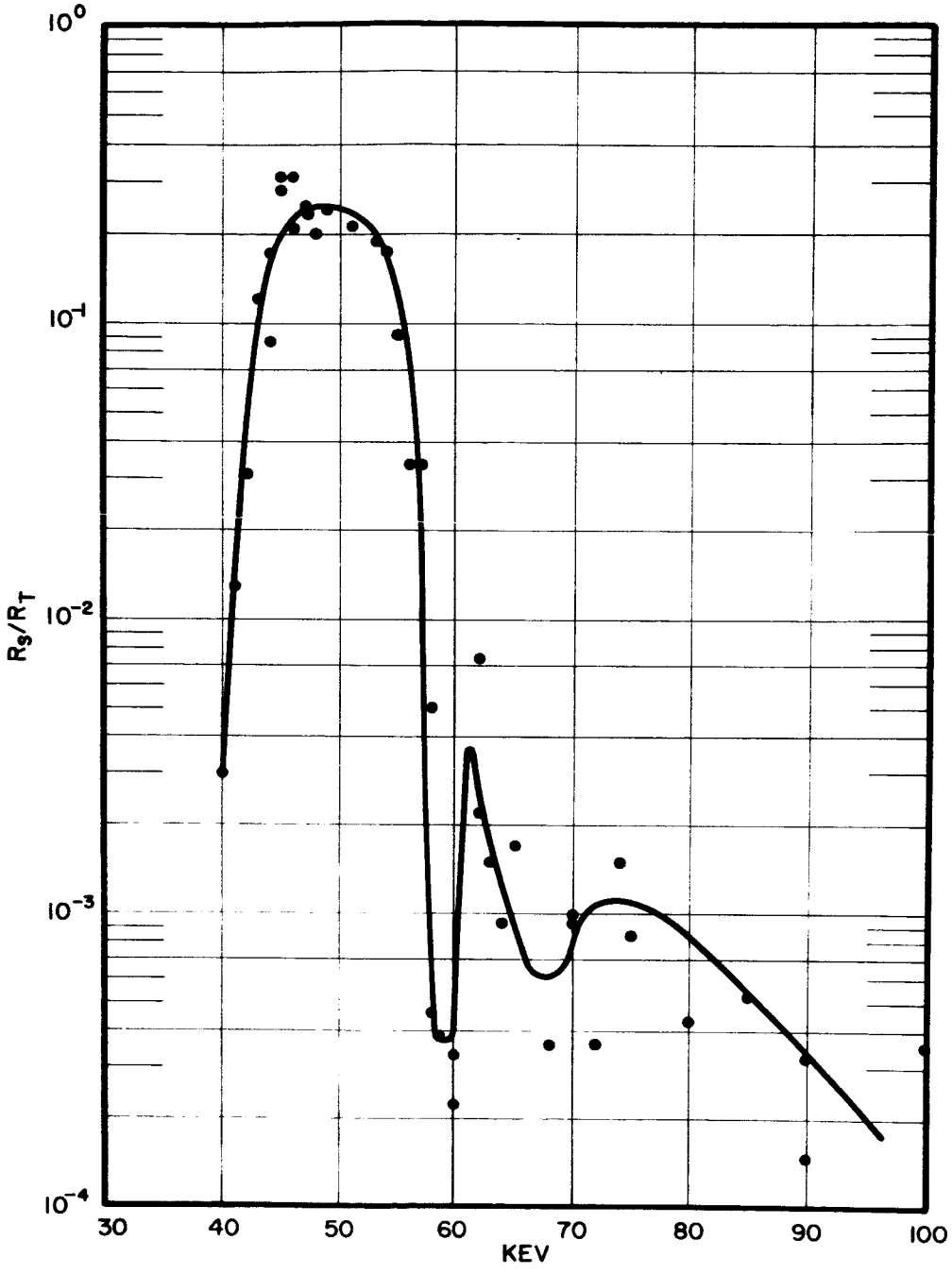

FIG. 16, R_S/R_T VS. ELECTRON ENERGY FOR UNIT NO. 5

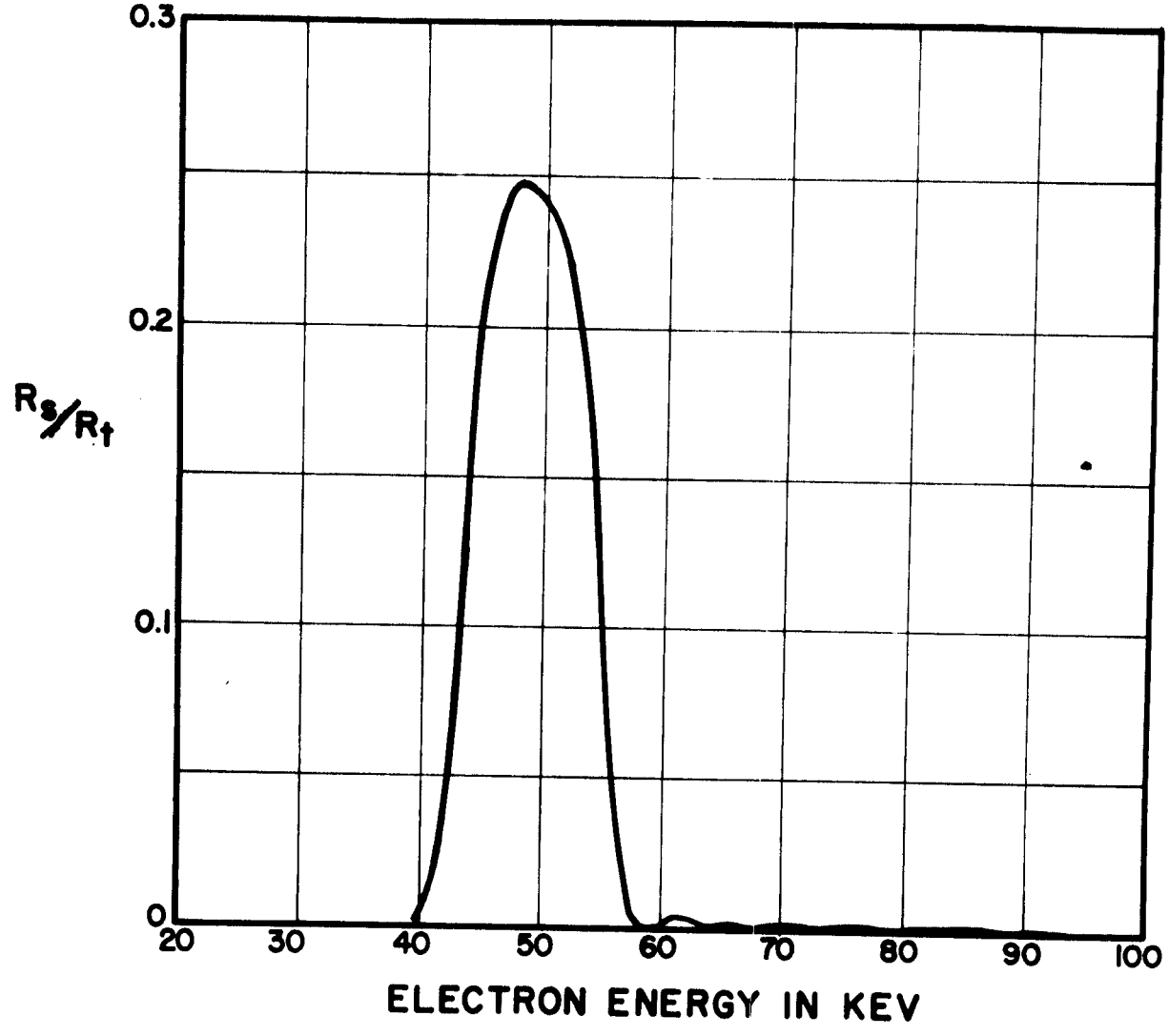

R_s/R_t vs. ELECTRON ENERGY FOR UNIT NO. 5.

FIG. 17

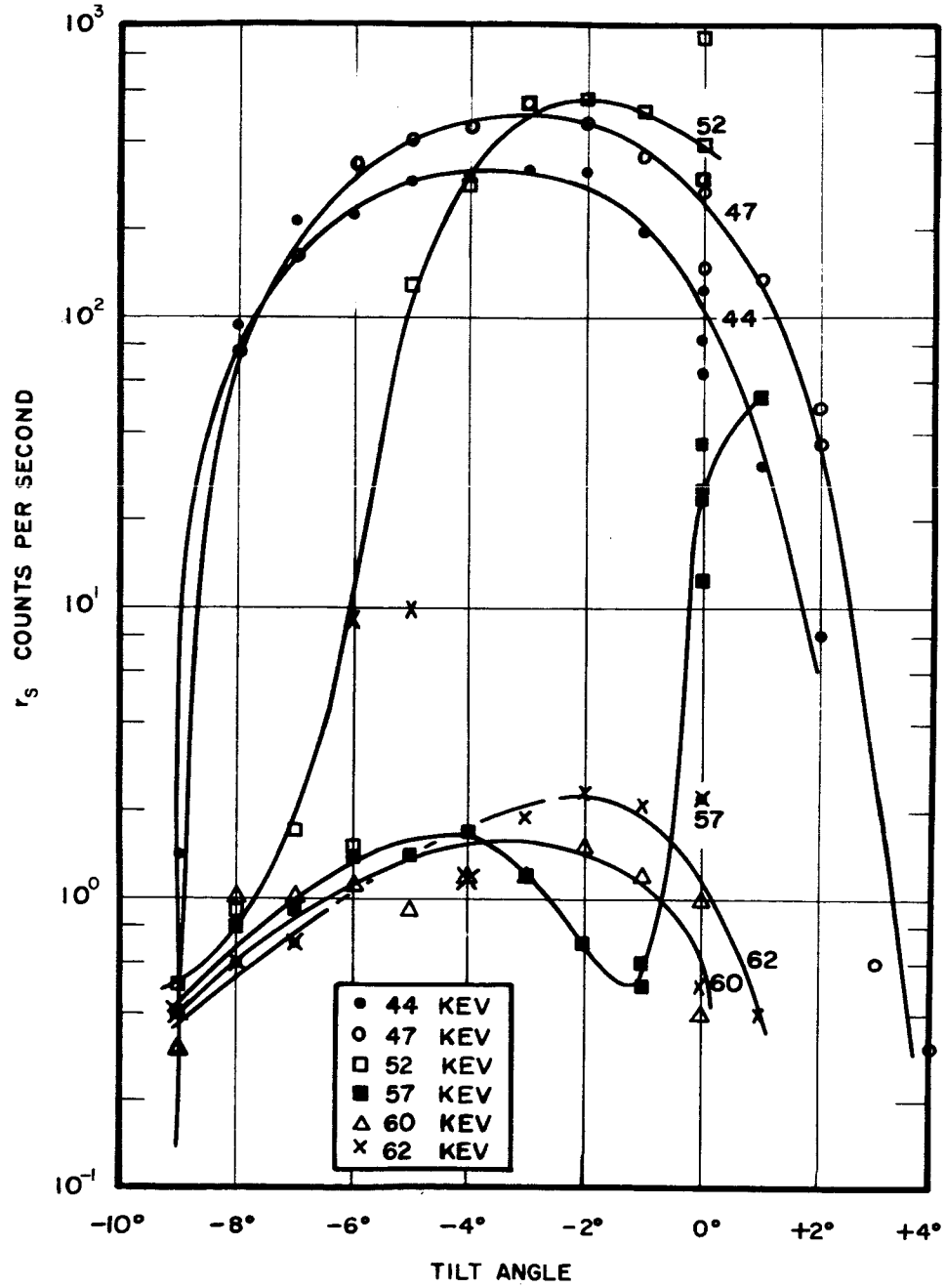

FIG. 18, r_s VS. TILT ANGLE FOR UNIT NO. 5

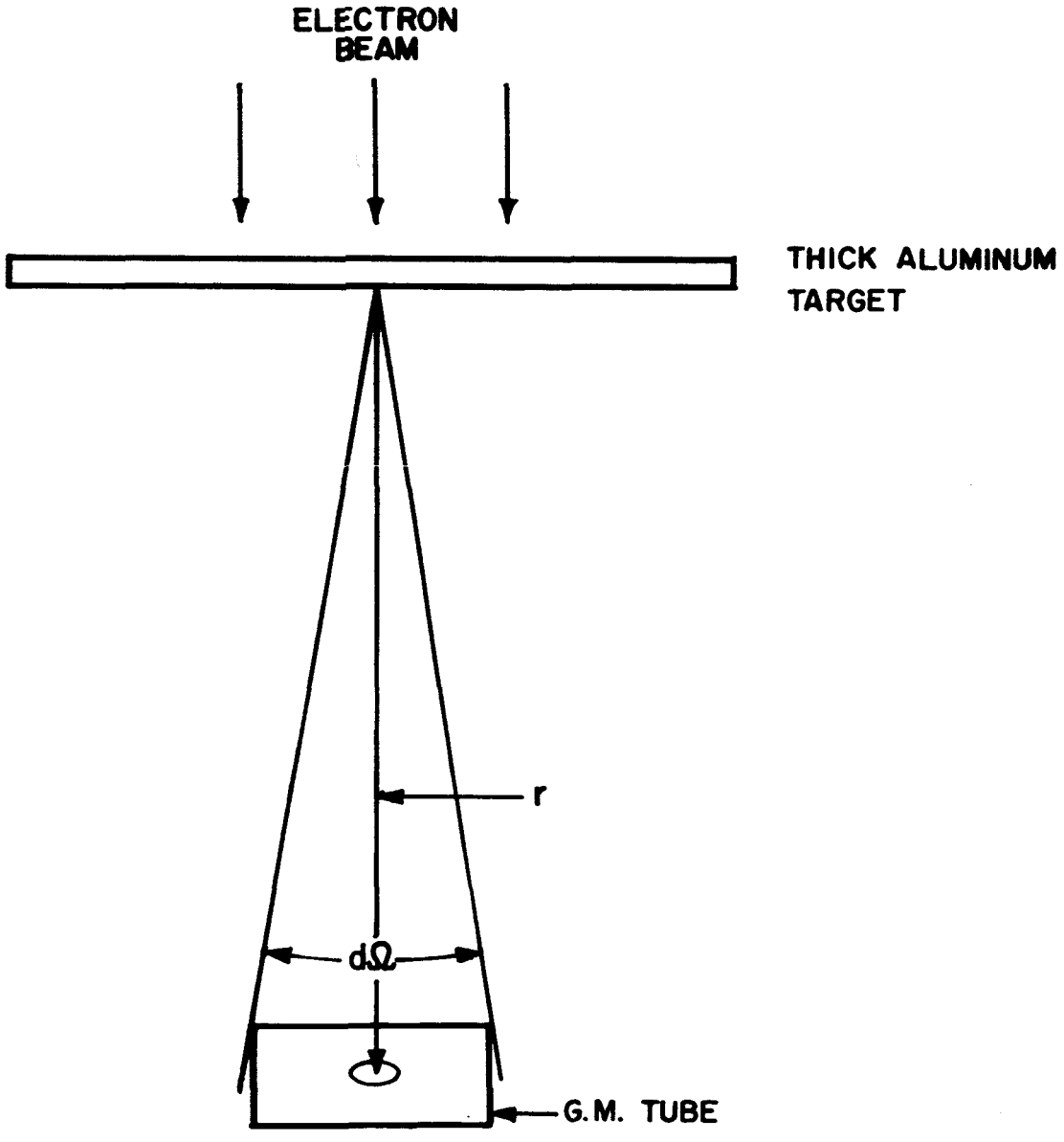

LABORATORY ARRANGEMENT FOR MEASURING BREMSSTRAHLUNG DETECTION

FIG. 19

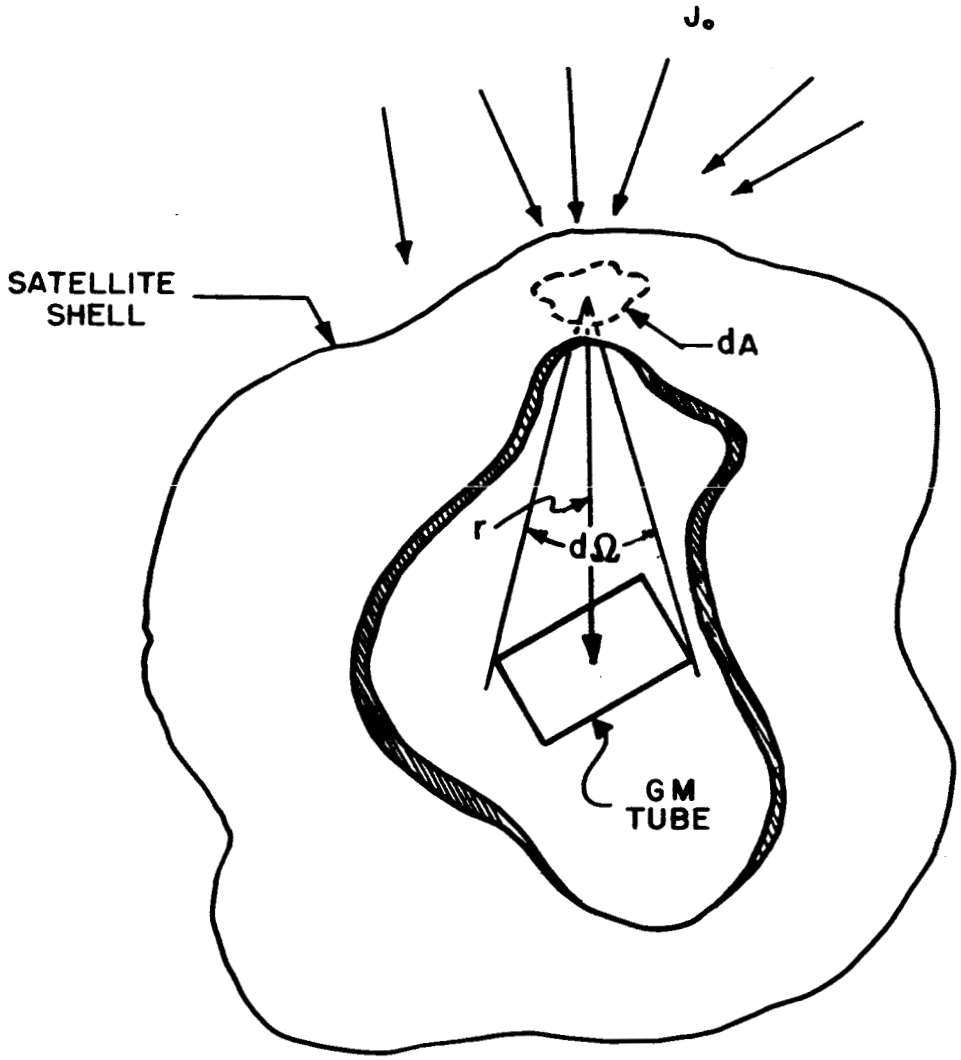

CONDITIONS FOR THE DETECTION OF BREMSSTRAHLUNG BY A GEIGER TUBE WITHIN A SATELLITE

FIG. 20

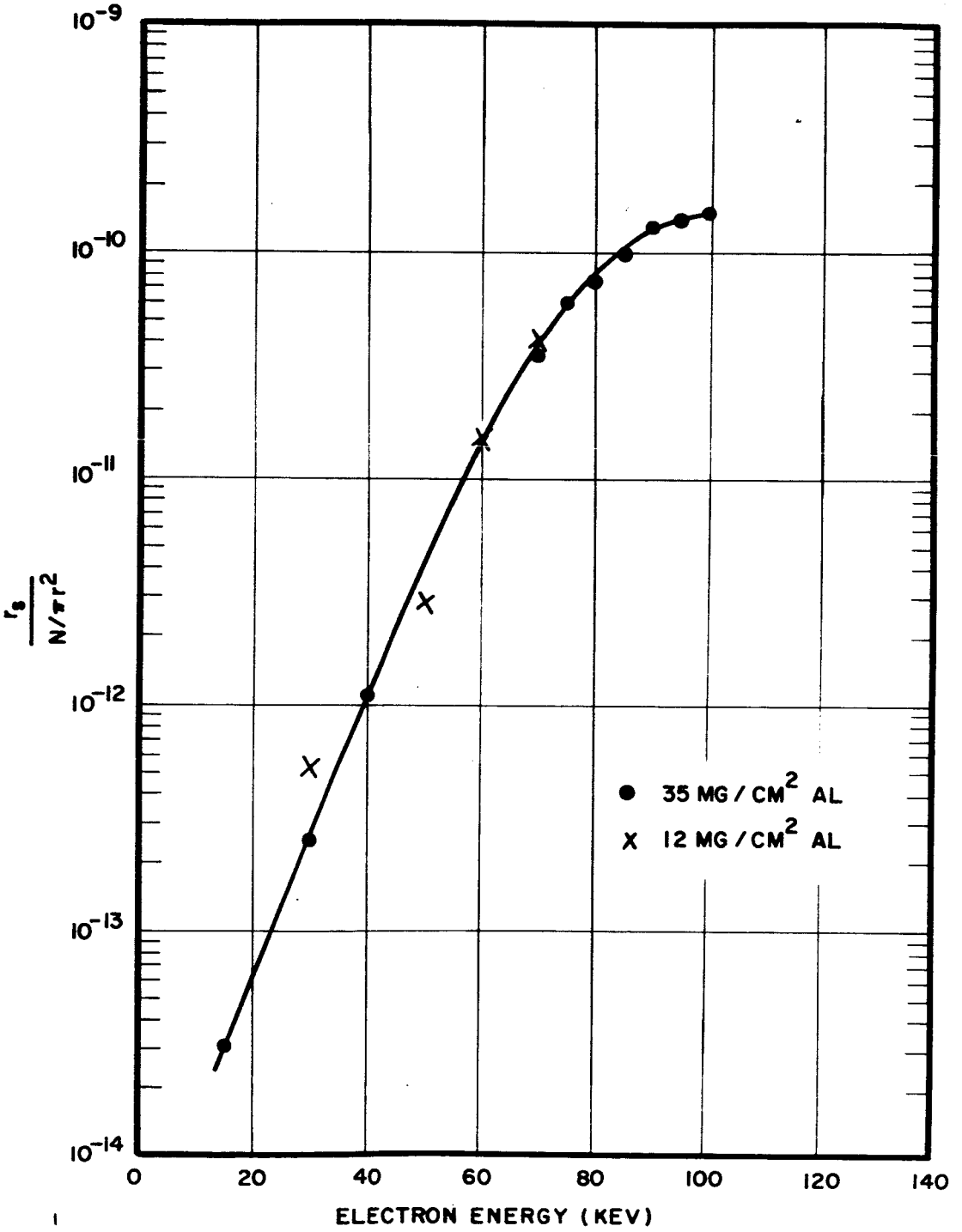

FIG. 21, COUNTS PER SECOND IN SPECTROMETER TUBE PER ELECTRONS CM^{-2} SEC^{-1} VS. ELECTRON ENERGY

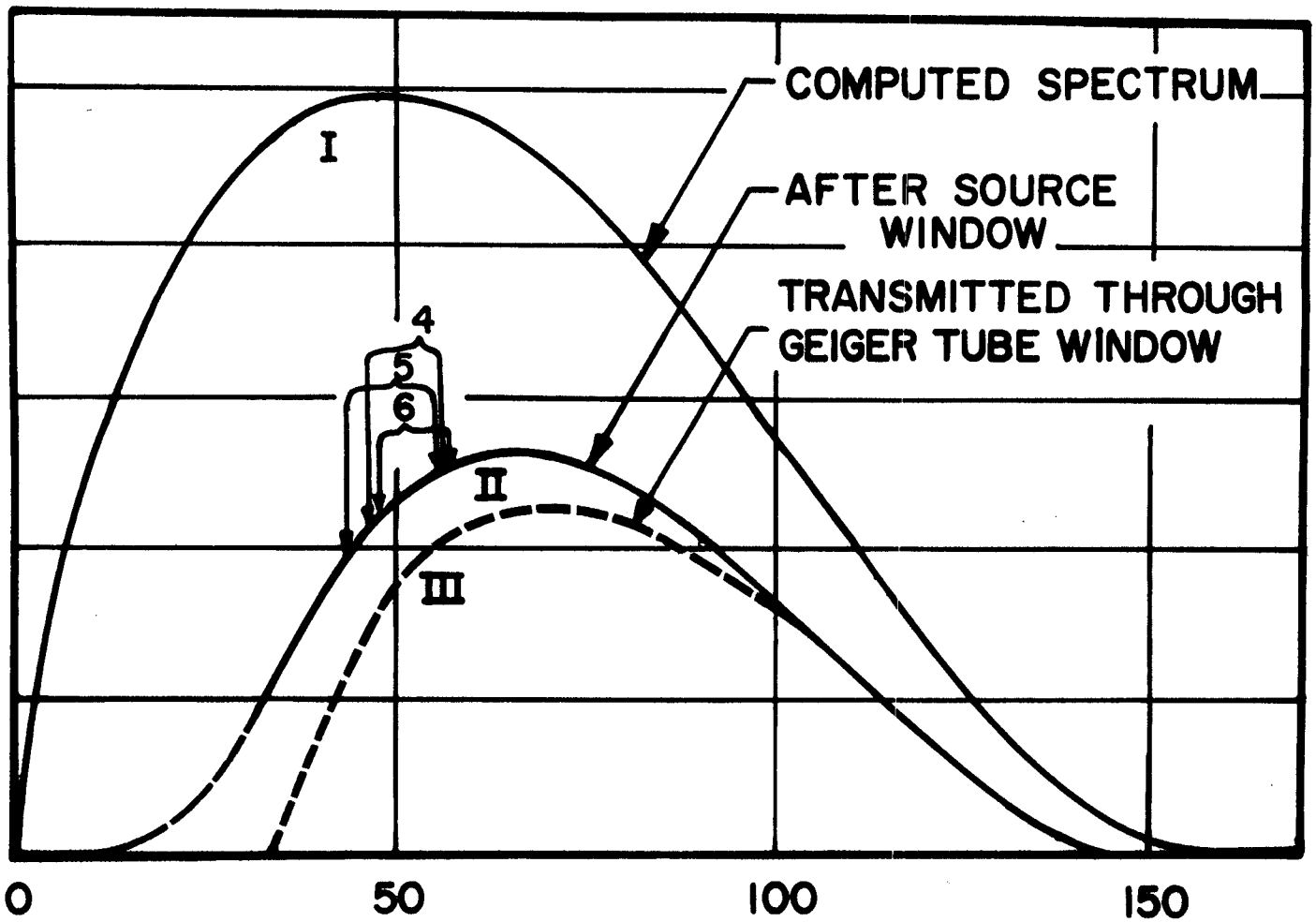

f (E) VS. E FOR $_{6}C^{14}$

FIG. 22

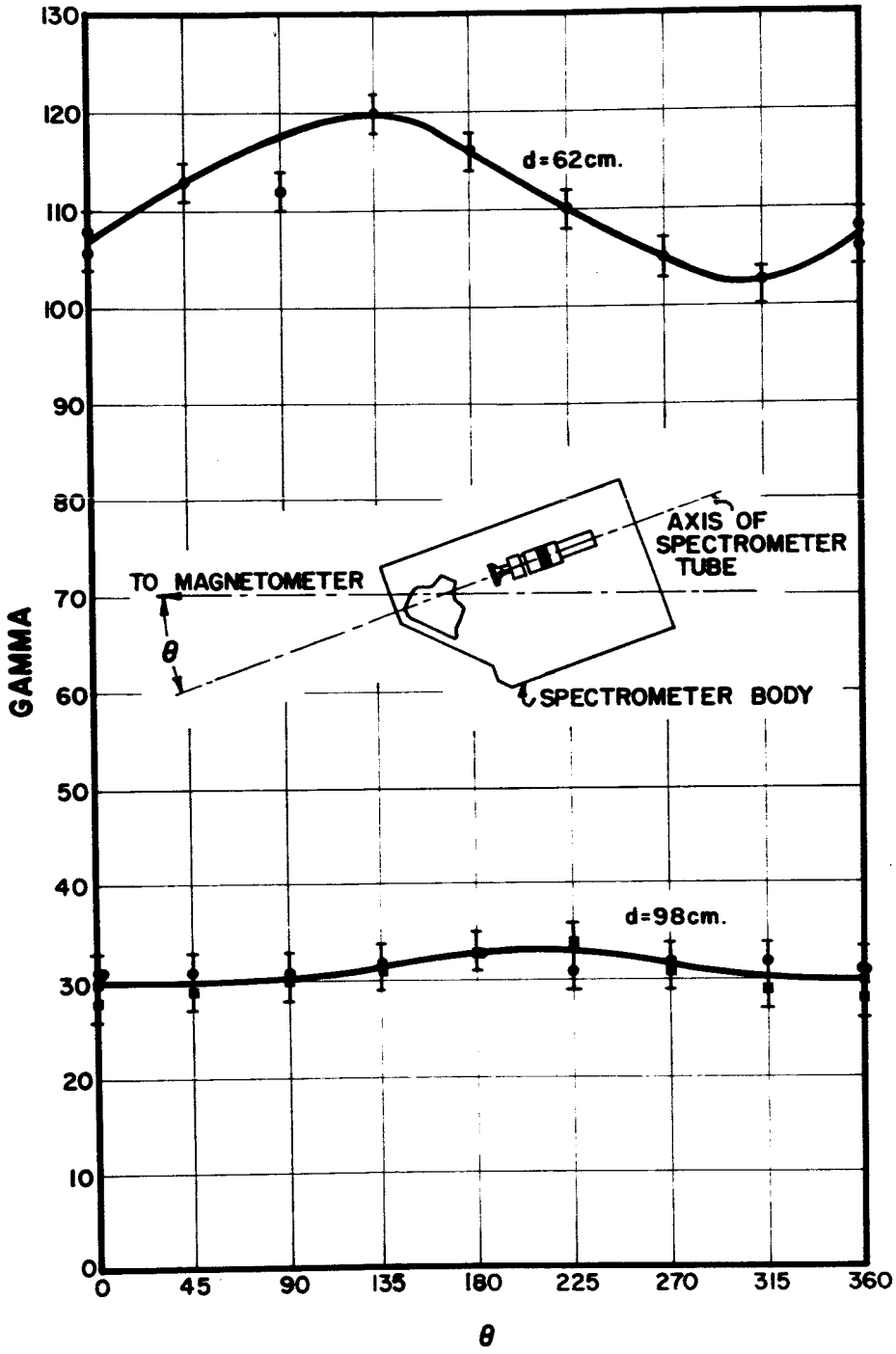

STRAY FIELD MEASURED IN THE PLANE OF THE GAP B=1050 GAUSS

FIG. 23